3

Dielectric Properties of Biological Materials

Camelia Gabriel

CONTENTS

3.1 Introduction

At some level of organization, all matter consists of charged entities held together by various atomic, molecular, and intermolecular forces. The effect of an externally applied electric field on the charge distribution is specific to the material; the dielectric properties are a measure of that effect; they are intrinsic properties of matter used to characterize nonmetallic materials. Biological matter has free and bound charges; an applied electric field will cause them to drift and displace, thus inducing conduction and polarization currents. Dielectric spectroscopy is the science that relates the dielectric properties to the underlying microscopic mechanisms of polarization and conduction. These dielectric phenomena are determined by and are informative about the structure and composition of the material. Consequently, knowledge of the dielectric properties is of practical importance in all fields of science where electromagnetic fields impinge or are used to probe or process matter. It is equally important in biomedical fields such as electrophysiology, where endogenous bioelectric sources provide signals that are sensed through various body tissues and are affected by their dielectric properties.

The past decade has seen a dramatic increase in the exposure of people to electromagnetic fields from wireless telecommunication devices and infrastructure. This situation sparked large research programs on the assessment and quantification of exposure of people and on the biological effects resulting from the exposure. Information on the dielectric properties of tissues is vital to these studies, for the computation of exposure metrics and the provision of a mechanistic explanation for biological effects. To satisfy the need of current research activity, this chapter will review the dielectric data for body tissue and the underlying mechanisms of interaction at the cellular, subcellular, and molecular levels. In doing so, we will draw on the authoritative article by Foster and Schwan (1996), published in the second edition of this book, which goes a long way toward establishing dielectric spectroscopy as a powerful tool for mechanistic studies.

Another area of scientific activity in the last decade revolved around the formulation of standard procedures for the experimental assessment of human exposure from electromagnetic sources, mostly telecommunication radio transceivers and their accessories. This created the need to formulate and measure the dielectric properties of tissue equivalent material and made dielectric measurement and the assessment of the associated uncertainty part of the compliance testing procedure. This chapter will deal with the fundamental issues that need to be established if dielectric measurement is to become a routine but accurate laboratory procedure.

It is not possible to review the dielectric properties and the polarization mechanisms in biological material without singling out the contribution to this field of Herman P. Schwan, whose name is associated with all the major findings over the past 50 years (Foster, 2002). Indeed, his 1957 review of the bulk electrical properties of cells and cell suspensions is one of the earliest and most studied texts on the subject. There are other reviews by Pethig (1979), Stuchly (1979), Schwan and Foster (1980), Pethig and Kell (1987), and Foster and Schwan (1989). The fundamental aspects and a more extensive treatment of the theoretical aspects of this subject can be found in books by Cole (1972), Grant et al. (1978), Schanne and Ceretti (1978), Pethig (1979), and more recently, Craig (1995), Roussy and Pearce (1995), and Grimnes and Martinsen (2000).

For most biological materials, the magnetic permeability is close to that of free space (i.e., diamagnetic), which implies that there is no direct interaction with the magnetic component of electromagnetic fields at low field strengths. However, this position is now changing following relatively recent reports of the presence of magnetite in human nervous tissue (see, e.g., Dobson and Grassi, 1996), which suggest that magnetite may provide a mechanism for direct interaction of external magnetic fields with the human central nervous system. The role of these strongly magnetic materials in organisms is only just beginning to be unraveled. This subject is elaborated in the second part of next chapter.

3.2 Dielectric Properties—Molecular Origin

From a historical perspective, the dielectric properties of materials were first observed experimentally by Faraday in the 1830s as a change in the capacity of an empty capacitor when a material is introduced inside it. Faraday introduced the term *specific inductive capacity* to describe the ratio of the capacities of the filled and empty capacitor. This quantity is now known as the permittivity and is denoted by ε. It is a fundamental property of nonmetallic or dielectric materials. Under quasistatic conditions, the capacitance C_0 of a perfect capacitor of area A and plate separation d changes to $C > C_0$:

$$C = \varepsilon\varepsilon_0 = \varepsilon\frac{\varepsilon_0 A}{d} \tag{3.1}$$

where ε is the relative permittivity of the material (dimensionless), ε_0 is the permittivity of free space (8.8542×10^{-12} F/m), and the product $\varepsilon\varepsilon_0$ is the absolute permittivity. The increase in capacity is due to the additional charge density induced by the field in the material. The field is said to have polarized the medium; polarizability or the ability of the material to polarize is the main determinant of its dielectric properties.

This section will start with the fundamental concepts of the interaction of homogenous matter with static fields and proceed, in steps, to heterogenous mixtures and their dynamic response to time-varying fields leading to the dielectric properties of tissues.

3.2.1 Quasi-Static Response

Considering the simple case of a monomolecular material, three main interaction mechanisms are possible: electronic, atomic, and molecular polarization. Electronic polarization is the shift of electrons, in the direction of the field, from their equilibrium position with respect to the positive nuclei. Atomic polarization is the relative displacement of

atoms or atom groups relative to each other. The orientation of permanent or induced molecular dipoles, when present, is known as molecular polarization. The total polarizability α_T is the sum of the contribution of, in this case, all three processes, termed α_e, α_a, and α_d.

In view of the relative importance of molecular orientation processes in defining the total polarization ($\alpha_e + \alpha_a < \alpha_d$) and hence the dielectric properties, it is usual to differentiate between the polar and nonpolar materials when these properties are considered.

For ideal nonpolar materials, the relationship $\varepsilon = n^2$, where n is the optical refractive index, holds true. When a dielectric material becomes polarized by the application of an external electric field E, the dipole moment of the constituent molecules is given by

$$\overline{m} = \alpha_T \overline{E}_l \tag{3.2}$$

where E_l is the local field acting on the molecules. The dipole moment per unit volume of the material P increases the total displacement flux density D, defined from the relationship $D = \varepsilon_0 E$ in vacuum and $D = \varepsilon_0 \varepsilon E$ in a medium of relative permittivity ε. The latter expression may also be written as

$$D = \varepsilon_0 E + P \tag{3.3}$$

The dependence of P on E can take several forms, the simplest and most common being a scalar proportionality:

$$P = \varepsilon_0 \chi E \tag{3.4}$$

where $\chi = \varepsilon - 1$ is the relative dielectric susceptibility. This simple relationship is valid for a perfect isotropic dielectric, at low or moderate field intensities and at static or quasi-static field frequencies.

If the material contains N dipoles per unit volume, then

$$P = N\alpha_T E_l \tag{3.5}$$

and

$$\varepsilon - 1 = \frac{N\alpha_T}{\varepsilon_0} \frac{E_l}{E} \tag{3.6}$$

The molecular description of the permittivity requires that the relationship between the microscopic and the macroscopic field intensities be known. In most cases, there is no exact solution to this problem, only more or less good approximations that hold within the confines of the assumptions and simplifications made, as will be briefly illustrated for typical classes of materials.

3.2.2 Permittivity of Low-Pressure Gases

At low pressures the molecules are far apart from each other, and their interaction with each other may be assumed to be negligible in comparison with the macroscopic field intensity E. Under these conditions $E_l \approx E$ and

$$\varepsilon - 1 = \frac{N\alpha_T}{\varepsilon_0} \tag{3.7}$$

The relative permittivity of a nonpolar gas is very close to 1, typically of the order of 1.0001 at atmospheric pressure.

3.2.3 Permittivity of Liquids and Dense Gases

When the intermolecular interactions are such that $E_l \neq E$, the local field must be estimated. One approach is to consider a spherical region inside the dielectric that is large compared to the size of a molecule; the field inside it is estimated for nonpolar materials to be

$$E_l = \left(\frac{\varepsilon + 2}{3}\right) E \tag{3.8}$$

which yields

$$\frac{3(\varepsilon - 1)}{\varepsilon + 2} = \frac{N}{\varepsilon_0}\alpha_T \tag{3.9}$$

The above expression is known as the Claussius–Mossoti–Lorentz formulation. It is not always valid, such as when the density of the material corresponds to $N = 3\ \varepsilon_0/\alpha_T$. An alternative formulation, valid when the molecules are polarizable point dipoles of permanent moment μ, was provided by Onsager:

$$\frac{(\varepsilon - n^2)(2\varepsilon + n^2)}{\varepsilon(n^2 + 2)^2} = \frac{N\mu^2}{9kT\varepsilon_0} \tag{3.10}$$

where k is the Boltzman constant and T is the absolute temperature.

Debye separated out the contribution to the total polarization of the permanent dipole from those associated with electronic and atomic displacements and arrived at the following relationship

$$\frac{\varepsilon - 1}{\varepsilon + 2} = \frac{N}{3\varepsilon_0}(\alpha + \mu^2/3kT) \tag{3.11}$$

While Onsager and Debye used semistatistical techniques to estimate the local field, others like Kirkwood, and later Fröhlich, used statistical methods to obtain a rigorous expression of the permittivity after taking local interactions into consideration and obtained

$$\frac{(\varepsilon - 1)(2\varepsilon + 1)}{3\varepsilon} = \frac{N}{\varepsilon_0}(\alpha + g\mu^2/3kT) \tag{3.12}$$

This is Kirkwood's equation for permittivity in which g is known as the Kirkwood correlation parameter, introduced to account for the effect of local ordering in the material. Fröhlich's theory gives

$$\frac{(\varepsilon - n^2)(2\varepsilon + n^2)}{\varepsilon(n^2 + 2)^2} = \frac{Ng\mu^2}{9kT\varepsilon_0} \tag{3.13}$$

which, except for the correlation parameter g, is identical to Onsager's equation.

This brief outline of the dielectric theory gives an idea of the nature of the electric field interaction problems and of the various techniques used to partially solve them under static field conditions. The solutions hold for slow time-varying fields as long as there is a quasistatic state. References to the original work by Debye (1929), Kirkwood (1936), Onsager (1936), and Fröhlich (1955) are given in Böttcher and Bordewijk (1978) and other well-known texts (Hill et al., 1969; Jonscher, 1983).

3.3 Time and Frequency Dependence of the Dielectric Response

Much of the interest in the dielectric properties of biological materials is concerned with their response to time-varying electric fields. This can be explained by the same macroscopic variables used for the quasi-static state except for the introduction of a time dependence for the excitation and response. The general discussion will assume sinusoidal fields and linear and isotropic responses, nonsinusoidal fields and material anisotropy, and nonlinearity being special cases.

3.3.1 Time-Dependent Polarization—Impulse Response—Kramers–Krönig Relations

The following relationship holds irrespective of the polarization mechanism:

$$P(t) = D(t) - \varepsilon_0 E(t) \tag{3.14}$$

For an ideal dielectric material with no free charge, the polarization follows the pulse with a delay determined by the time constant of the polarization mechanism. Assuming a rate process, which is that the rate of polarization is proportional to the constantly decreasing number of unpolarized units, the simplest expression for the polarization is obtained from the solution of the first-order differential rate equation with constant coefficients and time constant τ, giving

$$P(t) = P(1 - \mathrm{e}^{-t/\tau}) \tag{3.15}$$

The decay of polarization is also an exponential function

$$P(t) = \mathrm{e}^{-t/\tau} \tag{3.16}$$

For a linear system, the response to a unit-step electric field is the impulse response $f(t)$ of the system. The response of the system to a time-dependent field can be obtained from summation in a convolution integral of the impulses corresponding to a sequence of elements making up the electric field. For a harmonic field and a causal, time-independent system, the Fourier transform exists and yields

$$P(\omega) = \varepsilon_0 \chi(\omega) E(\omega) \tag{3.17}$$

indicating that the dielectric susceptibility $\chi(\omega)$ is the Fourier transform of $f(t)$. In general, the susceptibility is a complex function reflecting the fact that it informs on the magnitude and phase of the polarization with respect to the polarizing field

$$\chi(\omega) = \chi' - \mathrm{j}\chi'' \tag{3.18}$$

The real and imaginary parts of $\chi(\omega)$ can be obtained from the separate parts of the Fourier transform:

$$\begin{aligned}\chi'(\omega) &= \int_{-\infty}^{+\infty} f(t)\cos(\omega t)\,\mathrm{d}t = \int_{0}^{+\infty} f(t)\cos(\omega t)\,\mathrm{d}t \\ \chi''(\omega) &= \int_{-\infty}^{+\infty} f(t)\sin(\omega t)\,\mathrm{d}t = \int_{0}^{+\infty} f(t)\sin(\omega t)\,\mathrm{d}t\end{aligned} \tag{3.19}$$

The limit of integration can be changed from $-\infty$ to 0 since $f(t)$ is causal.

The impulse response $f(t)$ defines the dielectric response, and conversely, knowledge of the complex susceptibility allows the determination of the impulse response by carrying out the reverse transformation, which gives $f(t)$ in terms of either $\chi'(\omega)$ or $\chi''(\omega)$:

$$\begin{aligned}f(t) &= (2/\pi)\int_{0}^{+\infty} \chi'(\omega)\cos(\omega t)\,\mathrm{d}\omega \\ f(t) &= (2/\pi)\int_{0}^{+\infty} \chi''(\omega)\sin(\omega t)\,\mathrm{d}\omega\end{aligned} \tag{3.20}$$

Eliminating $f(t)$ from the above equations gives an expression of $\chi'(\omega)$ in terms of $\chi''(\omega)$ and vice versa. Thus, there is a relationship between the real and imaginary parts of the complex susceptibility of any material, such that knowledge of either enables the other to be calculated. The expressions of real and imaginary parts of the susceptibility or permittivity in terms of each other are known as the Kramers–Krönig relations and have been derived as

$$\begin{aligned}\chi'(\omega) &= \chi'(\infty) + \frac{2}{\pi}\int_{0}^{\infty} \frac{u\chi''(u) - \omega\chi''(\omega)}{u^2 - \omega^2}\,\mathrm{d}u \\ \chi''(\omega) &= \frac{2}{\pi}\int_{0}^{\infty} \frac{\chi'(u) - \chi'(\omega)}{u^2 - \omega^2}\,\mathrm{d}u\end{aligned} \tag{3.21}$$

where u is a variable of integration. Recalling the relationship between relative dielectric susceptibility and relative permittivity $\chi = \varepsilon - 1$, the permittivity is a complex function given by

$$\hat{\varepsilon}(\omega) = \varepsilon'(\omega) - \mathrm{j}\varepsilon''(\omega) = (1 + \chi'(\omega) - \mathrm{j}\chi''(\omega)) \tag{3.22}$$

Thus, the Kramers–Krönig relations relate ε' to the complete spectrum of ε'' and vice versa. A clear account of their derivation can be found in Jonscher (1983).

3.3.2 Permittivity of a Polar Substance—The Debye Equation

When a step field E is applied to a polar dielectric material, the electronic and atomic polarizations are established almost instantaneously compared to the time scale of the

molecular orientation; the total polarization reaches a steady state as a first-order process characterized by the time constant of the dipolar rotation. When the field is removed, the process is reversed; electronic and atomic polarizations subside first, followed by a relatively slow decay in dipolar polarization (Figure 3.1). The time constant τ depends on the physical process, in this case the rotational dynamics of the dipole determined by the size, shape, and intermolecular relations of the molecules. If P_∞ and P_0 are the instantaneous and steady-state polarization, respectively, then the total polarization for a first-order process characterized by a time constant τ is

$$P = P_\infty + (P_0 - P_\infty)(1 - \mathrm{e}^{-t/\tau}) \tag{3.23}$$

In time-varying fields the permittivity is a complex function originating from the magnitude and phase shift of the polarization with respect to the polarizing field:

$$\hat{\varepsilon} = \varepsilon' - \mathrm{j}\varepsilon'' = \varepsilon' - \mathrm{j}\sigma/\omega\varepsilon_0 \tag{3.24}$$

The real part ε' is a measure of the induced polarization per unit field and the imaginary part ε'' is the out-of-phase loss factor associated with it. The loss factor can also be represented by a conductivity term $\sigma = \omega\varepsilon_0\varepsilon''$ where ω is the angular frequency. The SI unit of conductivity is siemens per meter (S/m).

The frequency response of the first-order system is obtained from the Laplace transformation, which provides the relationship known as the Debye equation:

$$\hat{\varepsilon} = \varepsilon_\infty + \frac{(\varepsilon_0 - \varepsilon_\infty)}{1 + \mathrm{j}\omega\tau} = \varepsilon' - \mathrm{j}\varepsilon'' \tag{3.25}$$

The limiting values of the permittivity, ε_s and ε_∞, are known as static and infinite permittivity, respectively. The relaxation time τ corresponds to a relaxation frequency $f_\mathrm{r} = 1/2\pi\tau$. For a highly associated liquid such as water, the static permittivity can be expressed in terms of molecular parameters in accordance with the discussions in the previous section as

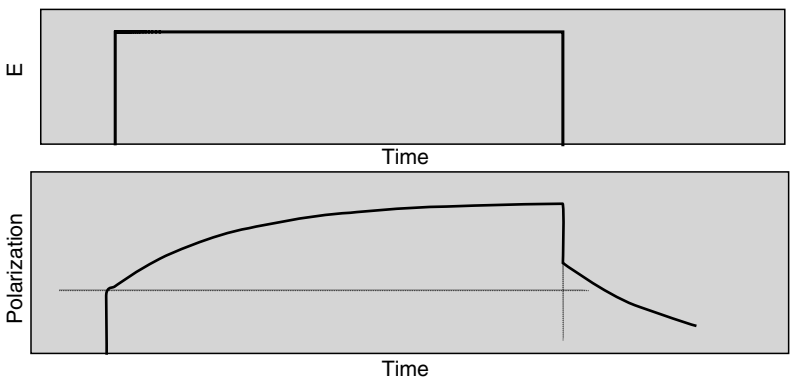

FIGURE 3.1
Schematic graph of dielectric response of a polar material expressed as polarization in the time domain in response to the step onset and removal of a polarizing electric field E. The nearly instantaneous rise in polarization, indicated by the horizontal dotted line, is P_∞; the vertical dotted line marks the instant and equivalent drop in polarization occurs when the field is removed.

$$\varepsilon_s = \varepsilon_\infty + \frac{Ng\mu^2}{2kT\varepsilon_0} \tag{3.26}$$

The relaxation time may be identified with the time constant of the molecular polarization and expressed in terms of molecular parameters. If η is the viscosity, then for a spherical molecule of radius a

$$\tau = 4\pi a^3 \eta / kT \tag{3.27}$$

For most polar materials, though not for water, ε_∞ corresponds to the optical permittivity and is equal to the square of optical refractive index n of the medium:

$$\varepsilon_\infty = n^2 \tag{3.28}$$

The dielectric properties of polar molecules vary with temperature; in general, both ε_s and τ decrease with increasing temperature.

As with the charge density and polarization, the time dependence of the current density J and σ, the current density per unit field, also follows a first-order law such that

$$J/E = \sigma_\infty + (\sigma_s - \sigma_\infty)(1 - e^{-t/\tau}) \tag{3.29}$$

This transforms into the conductivity equivalent of the Debye equation:

$$\hat{\sigma} = \sigma_\infty + \frac{(\sigma_s - \sigma_\infty)}{1 + j\omega\tau} \tag{3.30}$$

Figure 3.2 shows the variation in the permittivity, loss factor, and conductivity with frequency for a single time constant relaxation; such behavior pertains to an idealized monomolecular polar substance with no residual frequency-independent conductivity, that is $\sigma_s = 0$. The best, if not the only, example of such material is pure water as will be discussed later.

At the relaxation frequency, the permittivity is halfway between its limiting values and the loss factor at its highest. In the case of a single time constant as described in Figure 3.2, the conductivity is halfway between its limiting values at the relaxation frequency.

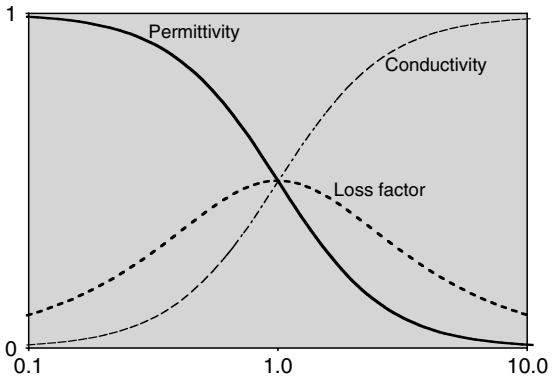

FIGURE 3.2
Normalized permittivity $(\varepsilon' - \varepsilon_\infty)/(\varepsilon_s - \varepsilon_\infty)$, loss factor $\varepsilon''/(\varepsilon_s - \varepsilon_\infty)$, and conductivity $\omega\varepsilon_0\,\varepsilon''/(\varepsilon_s - \varepsilon_\infty)$ for a single time constant relaxation plotted against f/f_r.

3.3.3 Nonpolar Molecules

The permittivity of nonpolar materials is virtually constant throughout the frequency range. In general, the temperature dependence is not significant. The static and optical values of the permittivity are almost identical, hence the Maxwell relation $\varepsilon = n^2$ holds true throughout the frequency and temperature range.

3.4 Observed Responses of Real Systems—Conduction—Multiple Relaxations—The Universal Law

In the previous section we described the expected behavior of idealized materials; we now need to deal with the observed responses of real systems. Few materials exhibit single relaxation time dispersions as in the Debye model; real materials depart from this ideal behavior to a greater or lesser extent depending on the complexity of the underlying mechanisms. To describe these responses we need to introduce the concepts of multiple dispersions and distribution of relaxation time. Moreover, biological materials exhibit conduction as well as polarization mechanisms; this needs to be taken into consideration in describing their dielectric response.

3.4.1 Conduction

The Debye expression does not include the effect of conduction currents as would arise from, for example, the drift of free ions in static fields. If σ_s is the static conductivity, the Debye expression becomes

$$\hat{\varepsilon} = \varepsilon_\infty + \frac{(\varepsilon_s - \varepsilon_\infty)}{1 - j\omega\tau} - \frac{j\sigma_s}{\omega\varepsilon_0} \tag{3.31}$$

In terms of real and imaginary parts we have

$$\begin{aligned} \varepsilon' &= \varepsilon_\infty + \frac{(\varepsilon_s - \varepsilon_\infty)}{1 + (\omega\tau)^2} \\ \varepsilon'' &= \frac{\sigma_s}{\omega\varepsilon_0} + \frac{(\varepsilon_s - \varepsilon_\infty)\omega\tau}{1 + (\omega\tau)^2} \end{aligned} \tag{3.32}$$

The total conductivity σ is given by

$$\sigma = \omega\varepsilon_0\varepsilon'' = \sigma_s + \frac{(\varepsilon_s - \varepsilon_\infty)\varepsilon_0\omega^2\tau}{1 + (\omega\tau)^2} \tag{3.33}$$

The total conductivity is thus made of two terms corresponding to the residual static conductivity and polarization losses. In practice, it is only possible to measure the total conductivity of a material; σ_s is obtained from data analysis or by measurement at frequencies corresponding to $\omega\tau \ll 1$ where the dipolar contribution to the total conductivity is negligible.

3.4.2 Multiple Relaxation Models—Distribution of Relaxation Times—Fractional Power Law Behavior

The occurrence of multiple interaction processes or the presence of more than one molecular conformational state or type of polar molecule may cause the dielectric behavior of a substance to exhibit multiple relaxation time dispersions. Deviation from Debye behavior may also indicate a polarization process whose kinetics are not first order or the presence of a complex intermolecular interaction. Models are needed to analyze the dielectric spectra of complex systems to unravel the underlying interaction mechanisms.

The simplest case is that of a dielectric response arising from multiple first-order processes; in this case the dielectric response will consist of multiple Debye terms to correspond to the polarization processes such that

$$\hat{\varepsilon} = \varepsilon_\infty + \frac{\Delta\varepsilon_1}{1 - j\omega\tau_1} + \frac{\Delta\varepsilon_2}{1 - j\omega\tau_2} + \cdots \tag{3.34}$$

where $\Delta\varepsilon_n$ corresponds to the limits of the dispersion characterized by time constant τ_n. If the relaxation times are well separated such that $\tau_1 \ll \tau_2 \ll \tau_3 \ll \cdots$, a plot of the dielectric properties as a function of frequency will exhibit clearly resolved dispersion regions.

If, as is quite often the case, the relaxation times are not well separated, the material will exhibit a broad dispersion encompassing all the relaxation times. In the limit of a continuous distribution of relaxation times, the multiple Debye expression would be

$$\hat{\varepsilon} = \varepsilon_\infty + (\varepsilon_s - \varepsilon_\infty) \int_0^\infty \frac{\rho(\tau)\, d\tau}{1 - j\omega\tau} \tag{3.35}$$

where

$$\int_0^\infty \rho(\tau)\, d\tau = 1 \tag{3.36}$$

The above equations can be used to represent all dielectric dispersion data, provided an appropriate distribution function $\rho(\tau)$ is available. Conversely, it should also be possible, at least in principle, to invert dielectric relaxation spectra to determine $\rho(\tau)$ directly; however, this is not easily achievable in practice. More commonly, one has to assume a distribution to describe the frequency dependence of the dielectric properties observed experimentally. The choice of distribution function should depend on the cause of the multiple dispersions in the material. For example, one can assume a Gaussian distribution as is known to occur for other physical characteristics (Figure 3.3) would be

$$\rho(t/\tau) = \frac{b}{\sqrt{\pi}} e^{-b^2[\ln(t/\tau)]^2} \tag{3.37}$$

where τ is the mean relaxation time. The shape of the Gaussian function depends on the parameter b; it reduces to the delta function when b tends to infinity and becomes very broad when b decreases; the area under the curve remains the same as required by the normalization condition. Incorporated into the expression for complex permittivity, it produces an expression that cannot be solved analytically, which makes it impractical for experimental data analysis.

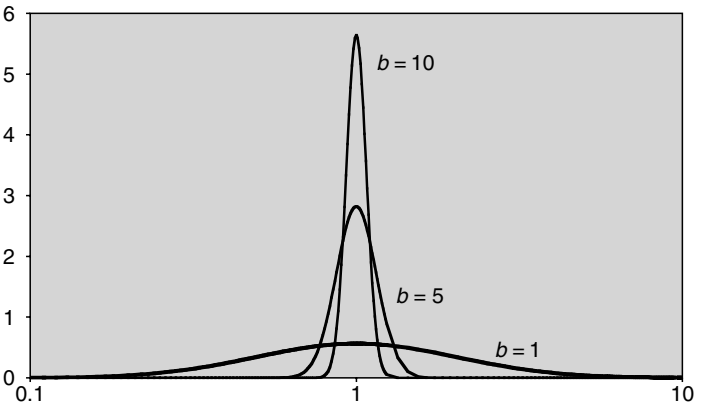

FIGURE 3.3
Gaussian distribution function as a function of t/τ.

Numerous empirical distribution functions or models have been proposed to model the experimental data without elaboration of the underlying mechanisms. One of the most commonly used models, a modified version of the Debye expression, was proposed in 1941 by Cole and Cole and is widely known as the Cole–Cole model:

$$\hat{\varepsilon} = \varepsilon_\infty + \frac{(\varepsilon_s - \varepsilon_\infty)}{1 - (j\omega\tau)^{1-\alpha}} = \varepsilon' - j\varepsilon'' \tag{3.38}$$

In it, α is a distribution parameter in the range $1 > \alpha \geq 0$; for $\alpha = 0$, the model reverts to the Debye equation. The real and imaginary parts are

$$\begin{aligned} \varepsilon' &= \varepsilon_\infty + \frac{(\varepsilon_s - \varepsilon_\infty)[1 - (\omega\tau)^{1-\alpha} \sin(\alpha\pi/2)]}{1 + (\omega\tau)^{2(1-\alpha)} + 2(\omega\tau)^{1-\alpha} \sin(\alpha\pi/2)} \\ \varepsilon'' &= \frac{(\varepsilon_s - \varepsilon_\infty)(\omega\tau)^{1-\alpha} \cos(\alpha\pi/2)}{1 + (\omega\tau)^{2(1-\alpha)} + 2(\omega\tau)^{1-\alpha} \sin(\alpha\pi/2)} \end{aligned} \tag{3.39}$$

Eliminating $\omega\,\tau$ from the above equations gives

$$\left(\varepsilon' - \frac{(\varepsilon_s + \varepsilon_\infty)}{2}\right)^2 + \left(\varepsilon'' + \frac{(\varepsilon_s + \varepsilon_\infty)}{2} \cot\frac{(1-\alpha)\pi}{2}\right)^2 = \left(\frac{\varepsilon_s - \varepsilon_\infty}{2} \operatorname{cosec}\frac{(1-\alpha)\pi}{2}\right)^2 \tag{3.40}$$

indicating that a plot of ε' against ε'' is a semicircle with its center below the real axis. For $\alpha = 0$, the Debye equivalent of the above equation is

$$\left(\varepsilon' - \frac{(\varepsilon_s + \varepsilon_\infty)}{2}\right)^2 + \varepsilon''^2 = \left(\frac{\varepsilon_s - \varepsilon_\infty}{2}\right)^2 \tag{3.41}$$

which indicates that ε' against ε'' is a semicircle with its center on the real axis (Figure 3.4); these semicircle plots are known as Cole–Coles.

The distribution function that corresponds to the Cole–Cole model is

$$\rho(t/\tau) = \frac{1}{2\pi} \frac{\sin(\alpha\pi)}{\cos h[(1-\alpha)\ln(t/\tau)] - \cos(\alpha\pi)} \tag{3.42}$$

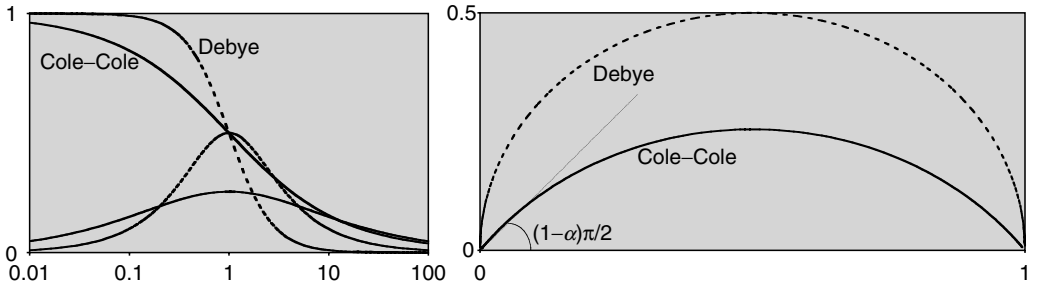

FIGURE 3.4
Left: Frequency dependence of normalized permittivity $(\varepsilon' - \varepsilon_\infty)/(\varepsilon_s - \varepsilon_\infty)$ and loss factor $\varepsilon''/(\varepsilon_s - \varepsilon_\infty)$ against frequency, normalized to the relaxation frequency, for a Debye and Cole–Cole with $\alpha = 0.4$. Right: Plot of normalized permittivity against loss factor showing a semicircle with its center on the real axis in the case of the Debye and an arc of a semicircle with its center below the real axis in the case of the Cole–Cole; the apex of the arc corresponds to the mean relaxation frequency.

Here again, τ is the mean relaxation time. As with the Gaussian, this distribution is logarithmically symmetrical about t/τ (Figure 3.5).

In 1951, Davidson and Cole proposed another variant of the Debye equation in which an exponent β is applied to the whole denominator:

$$\hat{\varepsilon} = \varepsilon_\infty + \frac{(\varepsilon_s - \varepsilon_\infty)}{(1 - j\omega\tau)^\beta} \tag{3.43}$$

which gives

$$\begin{aligned} \varepsilon' &= \varepsilon_\infty + (\varepsilon_s - \varepsilon_\infty)\cos(\beta\phi)(\cos\phi)^\beta \\ \varepsilon'' &= (\varepsilon_s - \varepsilon_\infty)\sin(\beta\phi)(\cos\phi)^\beta \end{aligned} \tag{3.44}$$

where $\phi = \arctan(\omega\tau)$. The corresponding distribution of relaxation times is

$$\rho(t/\tau) = \frac{1}{\pi}\left(\frac{t}{\tau - t}\right)^\beta \sin(\pi\beta) \tag{3.45}$$

When $\beta = 1$, the model reverts to the Debye equation. A plot of the real and imaginary parts of the model presents a skewed arc, similar to the Debye plot at low-frequencies, where it intercepts the abscissa at $\pi/2$, but at high frequencies the tangent to the arc is $\beta\pi/2$ (Figure 3.6).

The distribution function is shown graphically in Figure 3.7. It has a singularity at $t/\tau = 1$ and returns zero at $t > \tau$.

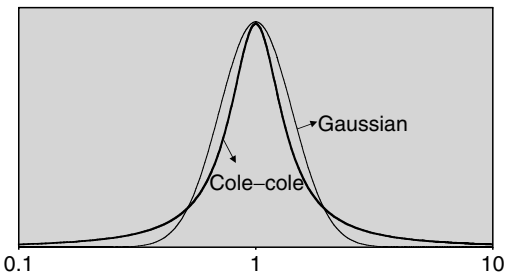

FIGURE 3.5
Gaussian distribution with $b = 2$ and Cole–Cole distribution with $\alpha = 0.09$ as a function of t/τ.

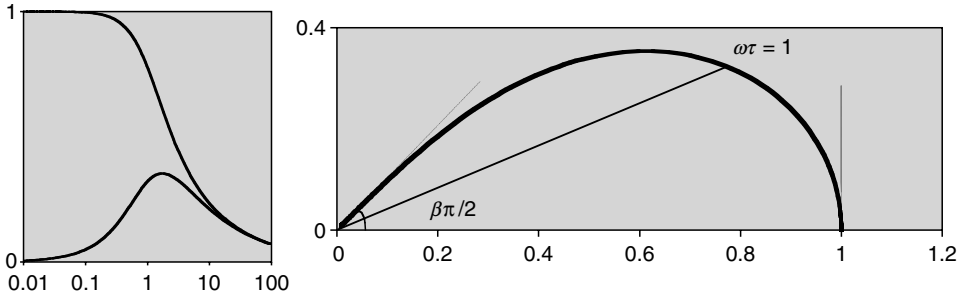

FIGURE 3.6
Left: Frequency dependence of normalized permittivity $(\varepsilon' - \varepsilon_\infty)/(\varepsilon_s - \varepsilon_\infty)$ and loss factor $\varepsilon''/(\varepsilon_s - \varepsilon_\infty)$ for a Cole–Davidson model with $\beta = 0.5$. Right: Plot of normalized loss factor against permittivity showing the characteristic Cole–Davidson skewed arc where the maximum in ε'' does not correspond with $\omega\tau = 1$; this point is found at the interception of the bisector of the high-frequency limiting angle with the data plot.

Another expression, sometimes used to model dielectric data, is the Havriliak–Negami relation (Havriliak and Negami, 1966). It combines the variations introduced in both the Cole–Cole and the Cole–Davidson models, giving

$$\hat{\varepsilon} = \varepsilon_\infty + \frac{(\varepsilon_s - \varepsilon_\infty)}{(1 - (j\omega\tau)^{(1-\alpha)})^\beta} \tag{3.46}$$

with real and imaginary parts:

$$\begin{aligned} \varepsilon' &= \varepsilon_\infty + \frac{(\varepsilon_s - \varepsilon_\infty)\cos(\beta\phi)}{1 + 2(\omega\tau)^{(1-\alpha)}\sin(\alpha\pi/2) + (\omega\tau)^{2(1-\alpha))^{\beta/2}}} \\ \varepsilon'' &= \frac{(\varepsilon_s - \varepsilon_\infty)\sin(\beta\phi)}{1 + 2(\omega\tau)^{(1-\alpha)}\sin(\alpha\pi/2) + (\omega\tau)^{2(1-\alpha))^{\beta/2}}} \end{aligned} \tag{3.47}$$

in which $\phi = \arctan\{[(\omega\tau)^{(1-\alpha)}\cos(\alpha\pi/2)]/[1 + (\omega\tau)^{(1-\alpha)}\sin(\alpha\pi/2)]\}$ and the corresponding distribution of relaxation times is

$$\rho(t/\tau) = \frac{1}{\pi}\frac{(t/\tau)^{\beta(1-\alpha)}\sin(\beta\theta)}{(t/\tau)^{2(1-\alpha)} + 2(t/\tau)^{(1-\alpha)}\cos(\pi(1-\alpha)) + 1)^{(\beta/2)}} \tag{3.48}$$

where $\theta = \arctan\{[(\sin(1-\alpha)\pi)/((t/\tau) + \cos(1-\alpha)\pi)]\}$.

The Cole–Cole plot of the Havriliak–Negami model is an asymmetric curve intercepting the real axis at different angles at high and low-frequencies (Figure 3.8). The distribution of relaxation times is also asymmetric (Figure 3.9).

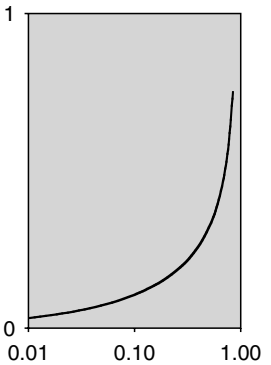

FIGURE 3.7
Cole–Davidson distribution with $\beta = 0.5$ as a function of t/τ.

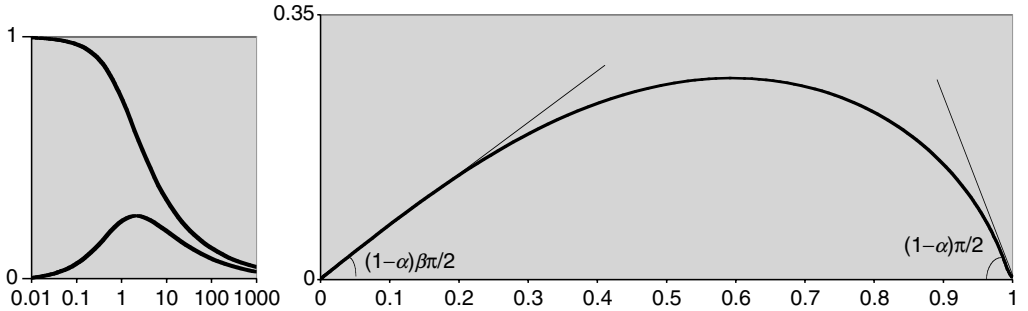

FIGURE 3.8
Left: frequency dependence of normalized permittivity $(\varepsilon' - \varepsilon_\infty)/(\varepsilon_s - \varepsilon_\infty)$ and loss factor $\varepsilon''/(\varepsilon_s - \varepsilon_\infty)$ for a Havriliak–Negami model with $\alpha = 0.2$ and $\beta = 0.5$. Right: Cole–Cole plot of the same data. As with the Cole-Davidson plot, the $\omega\tau = 1$ point is found at the interception of the bisector of the high-frequency limiting angle with the data plot.

Havriliak–Negami expressions revert to their Cole–Cole, Cole–Davidson, and Debye equivalents at the limiting values of β, α, and α and β, respectively. In principle, this should be the model of choice for dielectric data analysis. In practice, it is not widely used to describe the dielectric properties of biological material, as will be discussed later. It is important to recall that these empirical distribution functions lack mechanistic justification; however, they do serve a useful purpose in enabling the parametrization of the experimental data, albeit with very limited clarification of the underlying mechanisms.

Another limitation of this type of analysis is the possibility of obscuring multirelaxation processes, particularly the presence of a small amplitude dispersion following in the high-frequency tail end of a much larger principal one. This point is well illustrated by Wei and Sridhar (1993); they point out that a graphical representation of the parameter $\sigma'' = \omega\varepsilon_0(\varepsilon' - \varepsilon_\infty)$ versus $\sigma' = \omega\varepsilon_0\varepsilon''$ provides a more sensitive visualization of multirelaxation processes.

The Debye model and its many variations, including those described in this section, have been widely used over more than half a century primarily because they lend themselves to simple curve-fitting procedures. In particular, the Cole–Cole model is

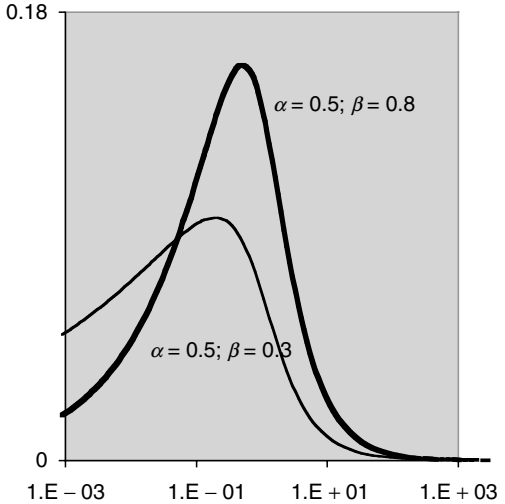

FIGURE 3.9
Havriliak–Negami distribution as a function of t/τ showing the effect of β for a given value of α.

used almost as a matter of course in the analysis of the dielectric properties of biological materials. Mathematically, at the limit of high frequencies, the Cole–Cole function simplifies to a fractional power law, that is, both ε' and ε'' are proportional to $(\omega\tau)^{(\alpha\ -1)}$. This fractional power law behavior is at the basis of what is known as the universal law of dielectric phenomena developed by Jonscher, Hill, and Dissado (Jonscher, 1983) for the analysis of the frequency dependence of dielectric data.

3.4.3 Universal Law of Dielectric Relaxation

Jonscher and his collaborators (Hill and Jonscher, 1983; Dissado and Hill, 1989) collated and analyzed extensive dielectric data obtained from numerous sources, pertaining to a wide range of materials, measured over a broad range of temperatures and frequencies. Their aim was to observe how dielectrics behave rather than presume a model for their frequency dependence; they studied the data on a log–log scale to better recognize the presence of a power law dependence, if present. Figure 3.10 shows plots for Debye and non-Debye responses where ω_p is the loss peak radial frequency.

Very few materials exhibit a pure Debye behavior where, at frequencies in excess of ω_p, the logarithmic slopes for $\varepsilon'(\omega)$ and $\varepsilon''(\omega)$ are -2 and -1, respectively, which is a Kramers–Krönig compatible result. However, for most materials a power law dependence of the type ω^{n-1}, with $n \neq 0$, applies for both $\varepsilon'(\omega)$ and $\varepsilon''(\omega)$. This is in compliance with the Kramers–Krönig relations, which require that at frequencies exceeding ω_p, both parameters follow the same frequency dependence, making the ratio $\varepsilon''(\omega)/\varepsilon'(\omega)$ frequency independent. Under such conditions, the ratio of energy dissipated to energy stored per radian of sinusoidal excitation is constant. The universal law can be summarized by the following frequency dependencies for the normalized complex permittivity:

$$\text{for } \omega < \omega_p, \quad \varepsilon''(\omega) \approx \omega^m \quad \text{and} \quad \varepsilon'(\omega) \approx 1 - \varepsilon''(\omega) \tag{3.49}$$

$$\text{for } \omega > \omega_p, \quad \varepsilon''(\omega) \approx \omega^{n-1} \quad \text{and} \quad \varepsilon'(\omega) \approx \varepsilon''(\omega) \approx \omega^{n-1} \tag{3.50}$$

Observation of the experimental data showed that ω_p is temperature dependent and follows an Arrhenius function:

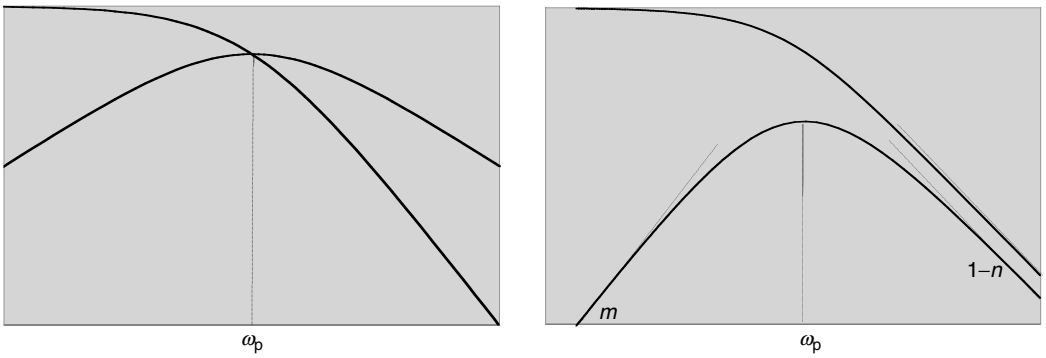

FIGURE 3.10
Log–log plot of the normalized permittivity and loss factor against frequency for a Debye-type behavior (left) and a non-Debye response (right).

$$\omega_{\mathrm{p}} = A\mathrm{e}^{-W/kT} \tag{3.51}$$

and the functional form for $\varepsilon''(\omega)$ is

$$\varepsilon''(\omega) = \frac{A}{(\omega/\omega_{\mathrm{p}})^{1-n} + (\omega_{\mathrm{p}}/\omega)^{\mathrm{m}}} \tag{3.52}$$

The values for $\varepsilon'(\omega)$ can then be determined numerically from the Kramer–Krönig relations.

Although the features of the dielectric spectra of most materials can be described using this approach, there is no theoretical justification for it. This makes it yet another empirical model, albeit a very general and mathematically elegant one.

3.4.4 Combined Response Model

A model that combines features from Debye-type and universal dielectric response behavior was proposed by Raicu (1999). In the course of modeling broad dielectric dispersions, as is often observed in the dielectric spectrum of biological materials, Raicu found that neither approach was good enough over a wide frequency range. He proposed the following very general function

$$\hat{\boldsymbol{\varepsilon}} = \boldsymbol{\varepsilon}_{\infty} + \frac{\Delta}{[(\mathrm{j}\omega\tau)^{\alpha} + (\mathrm{j}\omega\tau)^{1-\beta}]^{\gamma}} \tag{3.53}$$

where α, β, and γ are real constants in the range [0,1], τ is the characteristic relaxation time, and Δ is a dimensional constant, which becomes the dielectric increment $(\varepsilon_{\mathrm{s}} - \varepsilon_{\infty})$ when $\alpha = 0$, and the above expression reverts to the Havriliak–Negami model, which further reduces to the Debye, Cole–Cole, or Cole–Davison models with an appropriate choice of the α, β, and γ parameters. For $\gamma = 1$, it reverts to Jonsher's universal response model; in the special case where $\gamma = 1$ and $\alpha = 1 - \beta$, it becomes

$$\hat{\boldsymbol{\varepsilon}} = \boldsymbol{\varepsilon}_{\infty} + \left(\mathrm{j}\frac{\omega}{s}\right)^{\beta-1} \tag{3.54}$$

which is known as the constant phase angle model (Dissado, 1990). In this expression S is a scaling factor given by $S = (\Delta/2)^{1/(1-\beta)}\tau^{-1}$. The above expression was successfully used to model the dielectric spectrum of a biological material over five frequency decades from 10^3 Hz to 10^8 Hz.

3.5 Dielectric Properties of Biological Materials—Main Components

Tissue is a heterogenous material containing water, dissolved organic molecules, macromolecules, ions, and insoluble matter. The constituents are highly organized in cellular and subcellular structures forming macroscopic elements and soft and hard tissues. The presence of ions plays an important role in the interaction with an electric field, providing means for ionic conduction and polarization effects. Ionic charge drift creates conduction currents and also initiates polarization mechanisms through charge accumulation at

structural interfaces, which occur at various organizational levels. Their dielectric properties will thus reflect contributions to the polarization from both structure and composition. In this section, the contribution of each of the components will be determined individually and then collectively, leading to the formulation of models for the dielectric response of biological tissue.

3.5.1 Water

Water is a constituent of all living things; it is the environment in which body electrolytes and biomolecules reside and interact. Knowledge of its properties must precede the study of the more complex system. Many of the physical properties peculiar to water are due to its molecular asymmetry, polar nature, and ability to hydrogen bond, which are all interrelated. Water is described as an associated liquid because of its intermolecular hydrogen bonding. One practical reason for emphasizing the study of water in this chapter is its increasing use as a reference liquid, that is, a material of well-known dielectric properties. Consequently, it is often used as a standard for the calibration and testing of dielectric measuring procedures.

The dielectric properties of water are among the most studied and reported in the literature. Over the past decades, many experimental studies have been carried out to determine the dielectric properties of water over wide frequency and temperature ranges. These include Haggis et al. (1952), Lane and Saxton (1952), Hastead and El Sabeh (1953), Grant et al. (1957), Grant and Shack (1967), Grant and Sheppard (1974), Schwan et al. (1976), Grant et al. (1981), Hastead et al. (1985), Kaatze (1986, 1988), Buckmaster (1990), and Buchner et al. (1998). A comprehensive list of references and a historical overview of the subject can be found in Ellison et al. (1996). Other notable reviews were carried out by Kaatze (1989) and Liebe et al. (1991).

Data up to 100 GHz exhibit a near-perfect Debye dispersion with fairly well-defined parameters. Table 3.1 gives the Debye parameters for water at 20°C from three relatively recent reviews. Kaatze (1989) used a Debye expression to model his own extensive experimental data covering −4°C to 60°C and 1 to 57 GHz in addition to what he considered to be credible data from other sources.

Liebe et al. (1991) gathered extensive static and high-frequency data. For frequencies up to 100 GHz and temperatures from 0°C to 30°C, the data were a very good fit to the Debye function. However, including data at higher frequency somewhat reduced the goodness of the fit, suggesting the possible presence of a much smaller secondary dispersion in the hundreds of gigahertz range. The next logical step was then to use a two-Debye model. This proved a good fit to all experimental data up to 1 THz, thus confirming the presence of a small, high-frequency dispersion, probably due to some subtle molecular mechanism.

TABLE 3.1

Debye Parameters for Pure Water at 20°C

Review	ε_s	τ (ps)	ε_∞
Kaatze (1989)	80.2	9.47	5.2
Liebe et al. (1991)	80.1	9.35–9.39	5.3–5.4
Buchner et al. (1998)	80.2	9.32–9.52	5.9–6.0

Notes: For Liebe et al. (1991), τ and ε_∞ values are those of the single-Debye model (<100 GHz) and of the principal dispersion in the two-Debye model (up to 1 THz). Buchner et al. (1998) provide upper and lower bounds for τ and ε_∞ of the principal relaxation of a two-Debye model.

This secondary dispersion, centered around 670 GHz, brought down the high-frequency permittivity from 5.4 to 3.3 and made practically no impact on the characteristics of the principal dispersion, which were almost unchanged (Table 3.1). Liebe et al. (1991) extended the model to the far infrared (30 THz) by accounting for two near-infrared resonance absorption terms.

The most recent and comprehensive analysis of the dielectric properties of water is provided by Ellison et al. (1996), who critically reviewed the literature spanning the late 19th and most of the 20th centuries. With respect to the static permittivity, they obtained a function $\varepsilon_s = a\,e^{-b}$ with $a = 87.85306$ and $b = 0.00456992$, which predicts the value of ε_s at a given temperature to well within the limits of experimental accuracy for the range $-35^\circ C < t < 100^\circ C$. All high-frequency data (up to 1 THz) that met their selection criteria are tabulated. They stopped short of formulating models for the frequency dependence of the data; instead, they invited comments from the scientific community prior to the determination of what would probably be the ultimate model and spectral parameters for the dielectric properties of pure water, a finding that will greatly benefit this field of study. Already, other researchers have used this extensive survey. For example, Buchner et al. (1998) reported values for τ and ε_∞ of the principal water dispersion (Table 3.1) by fitting a two-Debye model to combined experimental data from Ellison et al. (1996) and other, more recent, studies (Barthel et al., 1995).

It is evident from Table 3.1 that the static permittivity and the relaxation time are fairly well-defined, less so the infinite permittivity. Fortunately, this parameter has little impact on the dielectric data in the gigahertz range because its value is only a small percentage of the permittivity in that frequency range. This relatively large uncertainty highlights the fact that even this most studied, pure substance is not a perfect reference liquid and that much remains to be done in the characterization of the dielectric properties of water at terahertz frequencies. Figure 3.11 is a plot of the dielectric properties of water at 20° tabulated by Ellison et al. (1996).

In biological materials, water is a solvent for salts, protein, nucleic acids, and smaller molecules. It is therefore important to study the effect of solutes on its dielectric response.

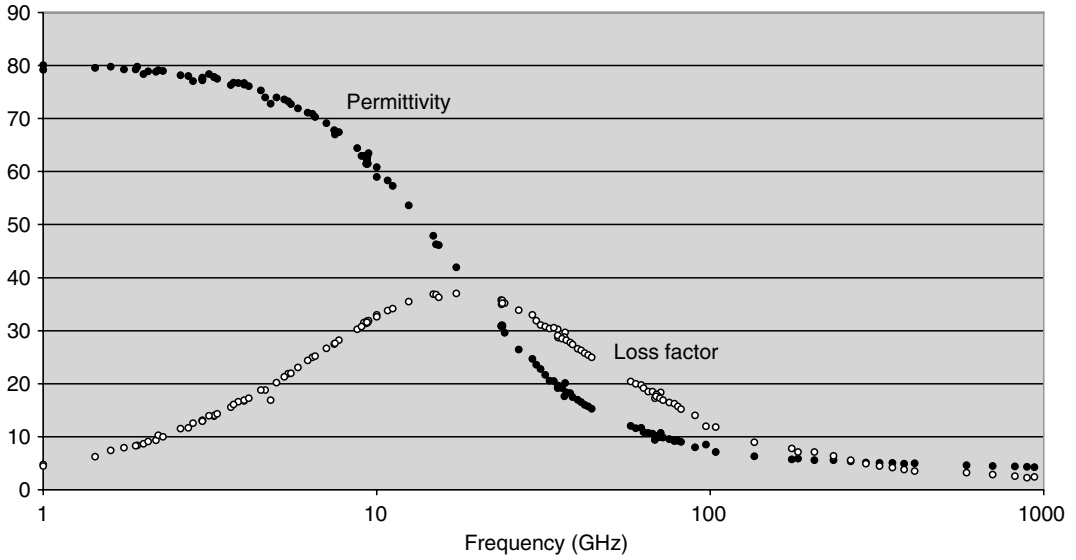

FIGURE 3.11
Experimental data from numerous sources reviewed and tabulated by Ellison et al. (1996).

3.5.2 Carbohydrates

In quantitative terms carbohydrates are not major constituents of animal cells; they are present at the surface of the cell membrane and are known to play a role in cellular communications. They are responsible for the gel consistency that gives certain body fluids such as vitreous humor and synovial fluid cushioning or lubricating properties. They are important constituents of certain tissues such as cartilage, tendon, and ligament. In terms of molecular structure, they vary in complexity and molecular size; they have in common the presence of one or more hydroxyl groups and the ability to hydrogen bond with each other or with water molecules. In aqueous solution they modify the principal dispersion of water to an extent that depends on the nature and concentration of the organic radical. In general, the dispersion is likely to be broader than a Debye, the static permittivity lower, and the relaxation time longer than for pure water, as observed and reported by Bateman and Gabriel (1987).

3.5.3 Proteins and Other Macromolecules

Protein constitutes the bulk of the organic matter in the body. Proteins are described as biopolymers, each molecule being a sequence of amino acids folded into a specific three-dimensional structure enclosing its hydrophobic sites within it. The surface has polar, hydrophilic groups with an affinity to bind water molecules from its surrounding aqueous environment. Part of the function of a protein resides in its structure; if the structure unfolds the protein is said to be denatured and is no longer functional. A good model for a globular protein in solution is that of a cluster of organic matter surrounded by a layer of strongly bound water; the solvent is referred to as free water to differentiate it from bound water. The size of the cluster depends on the molecular weight of the protein, which is typically of the order of tens or hundreds of thousands, that is, significantly larger than a water molecule. In an aqueous environment, most biological macromolecules including proteins act like polar molecules with permanent or induced dipole moment the magnitude of which depends on the molecular structure, configuration, and size.

Dielectric spectroscopy is therefore an important tool in the study of these molecular properties (Bateman et al., 1990, 1992). Typically, the dielectric dispersion of a protein will be in the megahertz frequency range, corresponding to a time constant of the order of microseconds. The dielectric spectrum of an aqueous globular protein solution will have two dispersion regions corresponding to the polarization of the protein and water molecules; the larger the protein the more clearly defined they will be. Conventionally, they are referred to as β and γ dispersions, respectively (Figure 3.12). Figure 3.12 shows a conceptual spectrum of a binary, protein–water system. In practice, to maintain the conformational stability of the biological molecules, inorganic ions, in the form of dissolved salts, must also be present. Table 3.2 has actual data, gathered from the literature, on the magnitude of the dielectric increment and the relaxation time for proteins of different shapes, sizes, and dipole moments. Many authors have reported the presence of a small dispersion that is attributed to bound water, described as molecules that are more or less strongly bound or otherwise affected by the presence of organic matter. When present, the spectral region of the bound water is termed δ dispersion. The book by Grant et al. (1978) is a good introduction to this important topic.

Larger biopolymers such as DNA, whose molecular weight may be of the order of several million, have more complex dielectric spectra with dispersions extending from kilohertz to megahertz. The elucidation of the polarization mechanisms responsible for

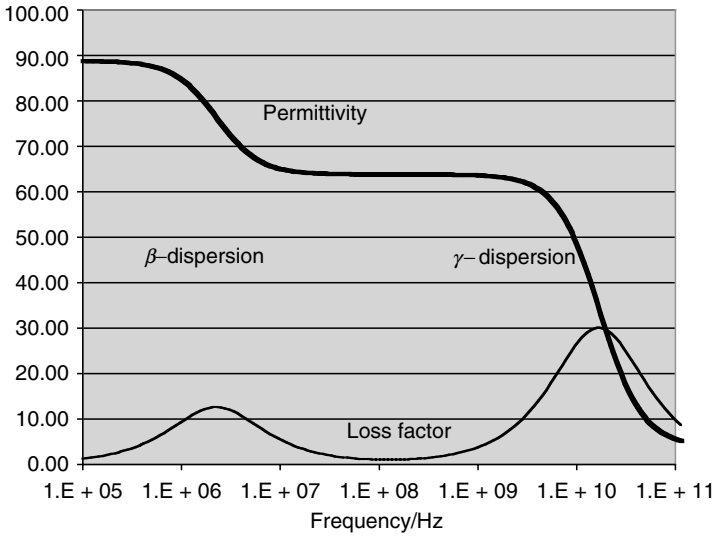

FIGURE 3.12
Conceptual representation of the dielectric spectrum of an aqueous protein solution. In practice, the two dispersions may overlap. The nearest to this picture is the complex permittivity spectrum of an aqueous solution of 1,2-dimyristoyl-L-3-phosphatidycholine reported by Kaatze and Giese (1980).

the dielectric spectrum of aqueous DNA solution is an area of active research. A good introduction to the subject is the book on biopolymers by Takashima (1989).

There is more than just academic interest in the study of biopolymers. Advances in nanotechnology are such that biological macromolecules are being considered as possible nanoscale electronic devices for fast information processing and transfer, a quest that will keep theoreticians and experimentalists busy for a long time.

3.5.4 Electrolytes

Electrolytes in the form of sodium, potassium, calcium, magnesium, chloride, and other ions play an important role in the function of biological systems. Many vital processes depend on a subtle balance being established between the concentration of electrolytes

TABLE 3.2

Dielectric Parameters of Various Proteins at 25°C

Protein	Mol wt. ($\times 10^3$)	$\Delta\varepsilon$	μ (D)	$\tau \times 10^8$ (s)	a/b
Myoglobin	17	0.15	170	2.9	—
β-Lactoglobulin (in 0.25 M glycine)	40	1.51	730	15, 5.1	4
Ovalbumin	44	0.10	250	18, 4.7	5
Horse carboxyhemoglobin	67	0.33	480	8.4	1.6
Horse serum albumin	70	0.17	380	36, 7.5	6
Horse serum pseudoglobulin	142	1.08	1100	250, 28	9

Notes: a/b is the axial ratio that determines the shape of the molecule. Where the shape deviates significantly from the spherical, two relaxation times are observed. The dielectric increment is $\Delta\varepsilon$, the dipole moment μ is given in Debye unit (1 D $= 3.33 \times 10^{-30}$ cm)
Source: From Foster KR, Schwan HP. 1989. *Crit Rev Biomed Eng* 17(1): 25–104. With permission.

inside and outside the cell. The cell membrane is, to a great extent, impermeable to the passive exchange of ions but allows directed movement under physiological control. In terms of dielectric properties, electrolytes have two effects. The direct effect, already mentioned, is the production of ohmic currents and energy loss in the system. This has the effect of making the static conductivity finite with a value commensurate with the ionic concentration and mobility. There are also important indirect effects whereby ionic charges contribute to the polarization of a biological system. One is interfacial polarization, whereby charge accumulation occurs at interfaces that are impermeable to ions. Another polarization mechanism is the ionic diffusion in electrical double layers adjacent to charged surfaces. Conduction, interfacial, and ion diffusion phenomena contribute significantly to the dielectric spectra of tissue.

3.5.5 Dielectric Dispersions in Tissue

The dielectric spectrum of a biological tissue (spleen at 37°C) is given in Figure 3.13 as an example of the response of a high water content tissue. Three main dispersion regions are immediately obvious and are referred to as α, β, and γ dispersions. The dispersions are rather broad, indicating the possible overlap of discrete relaxations arising from the polarization mechanisms encountered in the complex biological environment. Ionic conductivity contributes significantly to the loss factor, obliterating its features, and it is more

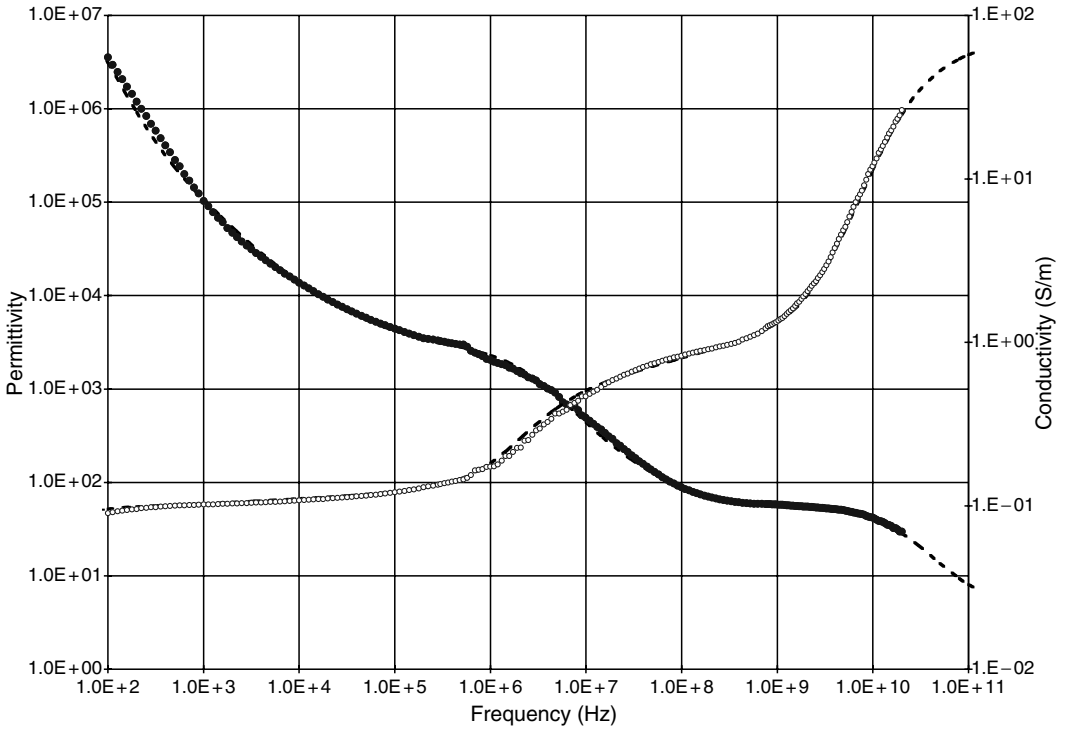

FIGURE 3.13
Dielectric spectrum of a high water content tissue (spleen at 37°C); experimental data are from Gabriel et al. (1996); dotted line is a best fit to a model of four Cole–Coles and a conductivity term.

informative to express the dielectric properties of tissues as permittivity and conductivity as in Figure 3.13.

3.5.5.1 α Dispersion

The α or low-frequency dispersion is characterized by very high permittivity values and can be ascribed, at least partially, to counterion diffusion effects. Such large dispersions are predicted by theories of ionic diffusion in heterogenous media. While it is not possible to model the complexity of a tissue, simpler mixture models predict dielectric increments of the right order of magnitude. Other mechanisms were postulated to contribute to the α dispersion; many relate to interactions in the vicinity of the cell membrane. The cell membrane is a complex, dynamic structure comprising a phospholipid bilayer. The lipid, hydrophobic ends of the phospholipids form a middle layer; the hydrophilic groups cover the inner and outer surfaces. Embedded in the bilayer are proteins, transport organelles, and ionic channels that operate under physiological control. The ionic balance between the intra- and extracellular media maintains a 60- to 70-mV potential difference between them of about 10 kV/mm across the membrane, assuming a 6- to 7-nm thickness. Membrane-related mechanisms that are thought to contribute to the α dispersion include the charging of intracellular membrane-bound organelles and a frequency dependence in the impedance of the cell membrane itself. An important reason for the uncertainty in the understanding of this dispersion is the paucity of error-free dielectric data in its frequency range. The α dispersion has a very large permittivity increment. The corresponding decrement in conductivity is small; this, however, does not contravene the principle of causality and the Kramers–Kronig relations, which predict a change in conductivity of about 0.005 S/m for a 10^6 increment in permittivity and relaxation frequency of 100 Hz.

3.5.5.2 β Dispersion

The β dispersion occurs at intermediate frequencies and originates mostly from the capacitive charging of the cellular membranes and those of membrane-bound intracellular bodies. This phenomenon, also known as interfacial polarization, has been studied theoretically and experimentally. It was established experimentally that damage to the cell membrane changes the features of the β dispersion. Numerous biomedical applications are based on the variation of the parameters of the β dispersion with pathological conditions involving changes in cell physiology and morphology. Tissue with directed, anisotropic cellular structure would exhibit an anisotropic dielectric response in the frequency range of the β dispersion.

Modeling the electrodynamics of a simplified tissue-like system, for example, suspensions of spherical inclusions in conductive media, has established theoretical grounds for the presence of the β dispersions. It enables the computation of an effective permittivity of similar order of magnitude to the β dispersion. For a system of concentric shells in conductive media (Hanai et al., 1988; Irimajiri et al., 1991), it predicts the presence of dielectric dispersions equal in number to the number of interfaces. These interfacial polarizations are boundary effects that occur in addition to other polarizations that may occur in the components of the system. The multiplicity of mehanisms goes a long way toward explaining why the β dispersions in tissue are rather broad.

3.5.5.3 γ Dispersion

The γ dispersion is due to the dipolar polarization of tissue water. At frequencies in excess of a few hundred megahertz, where the response of tissue water is the dominant

TABLE 3.3

Dielectric Parameters of Water Dispersion in Tissues Obtained by Analysis of Experimental Results at 37°C

Tissue	ε_s	τ (ps)	α	σ (S/m)
Bone (cortex)	14.9	13.8	0.26	0.092
Bone (section)	22.1	14.4	0.22	0.208
Cartilage	43.6	12.8	0.27	0.58
Cornea	53.0	8.72	0.13	1.05
Lens (cortex)	52.1	9.18	0.11	0.72
Lens (nucleus)	38.1	11.3	0.20	0.33
Retina	67.3	7.25	0.05	1.42
Brain (gray)	55.5	7.76	0.12	1.03
Brain (white)	37.0	8.04	0.24	0.47
Cerebellum	50.2	8.52	0.09	0.89
Dura	49.2	9.63	0.14	0.77
Brain stem	34.6	8.45	0.20	0.47
Tongue (*in vivo*)	57.7	9.12	0.08	0.63
Aqueous humor	74.2	6.81	0.01	1.83
Water	74.1	6.2	0.0	>0.0001

Source: From Gabriel et al. (1996c).

mechanism, the complex permittivity may be expressed as Cole–Cole plus a conductivity term to simulate the dipolar dispersion of water and the contribution of the electrolytes; thus,

$$\hat{\varepsilon}(\omega) = \varepsilon_\infty + \frac{\varepsilon_s - \varepsilon_\infty}{1 + (j\omega\tau)^{1-\alpha}} + \frac{\sigma}{j\omega\varepsilon_0}$$

where σ is the conductivity due to ionic currents and to the lower-frequency polarization mechanisms. Table 3.3 gives the parameters of the γ dispersion of tissues modeled to the above expression. The water content of the tissues considered ranges from >95% for vitreous humor and >85% for retina to <20% for cortical bone. The correlation between ε_s and tissue water content is an obvious and expected result. The value of the distribution parameter α is significant for most tissues and negligible for body fluids (as for aqueous humor, for example). The mean relaxation time τ is generally longer than the value for water, indicating a restriction in the rotational ability of at least some of the tissue water molecules. The lengthening of the relaxation time of water in biological material is a well-studied hypothesis; the effect is common to most organic solutes, is known to increase with solute concentration (Grant et al., 1981; Bateman et al., 1990), and has previously been observed in tissues (Gabriel et al., 1983).

3.5.5.4 δ Dispersion

Tissues and other biological materials may exhibit dispersions other than the three main ones. The δ dispersion, identified in some protein solutions between the β and γ, dispersions may also occur in tissue in the hundreds of megahertz range; when present, its magnitude is small compared to the adjacent ones. Possible mechanisms include the dipolar relaxation of bound water, relaxation of small dipolar segments or side chains of biological molecules, and counterion diffusion along small regions of the charged surface. Under these conditions it is difficult to isolate and, in view of the multiplicity of possible mechanisms, difficult to interpret. It is often treated as the tail end of the β dispersion or a broadening of the γ dispersion.

3.5.6 Effective Complex Permittivity of a Heterogenous System

Where adequate experimental data are available, the complex permittivity of a tissue can be quite adequately modeled with four Cole–Coles and a static conductivity term:

$$\hat{\varepsilon}(\omega) = \varepsilon_\infty + \sum_{n=1}^{4} \frac{\Delta\varepsilon_n}{1 + (\mathrm{j}\omega\tau_n)^{(1-\alpha_n)}} + \sigma_\mathrm{s}/\mathrm{j}\omega\varepsilon_0 \tag{3.55}$$

This is a descriptive model, imparting no definite information on the polarization mechanisms; the measured dielectric properties represent the bulk response of the tissue. Assigning effective parameters to a heterogenous medium is equivalent to treating it as homogenous where these parameters are concerned; in this case, its structural components are much finer than the wavelength of the field probing it.

The derivation of a general formula for the effective permittivity of a system in terms of those for its constituents is based on the theory of the transport properties of mixtures (Reynolds and Hough, 1957). For example, in the case of a binary mixture where a medium with permittivity ε_1 has inclusions of permittivity ε_2 and assuming that v_1 andv_2 are their respective volume fractions such that $v_1 + v_2 = 1$, then the average electric displacement D is given by

$$D = v_1 D_1 + v_2 D \tag{3.56}$$

and the average electric field is given by

$$E = v_1 E_1 + v_2 E_2 \tag{3.57}$$

The effective permittivity ε of the mixture is given by

$$D = \varepsilon\varepsilon_0 E \tag{3.58}$$

and for each component, $D_1 = \varepsilon_1\varepsilon_0 E_1$ and $D_2 = \varepsilon_2\varepsilon_0 E_2$. Equation 3.56 and Equation 3.57 give

$$\varepsilon = \varepsilon_1 v_1 f_1 + \varepsilon_2 v_2 f_2 \tag{3.59}$$

where $v_1 f_1 + v_2 f_2 = 1, f_1 = E_1/E$, and $f_2 = E_2/E$, which gives two general formulations for the effective permittivity of the mixture:

$$\varepsilon = \varepsilon_1 + (\varepsilon_2 - \varepsilon_1) v_2 f_2 \tag{3.60}$$

or

$$(\varepsilon - \varepsilon_1) v_1 f_1 + (\varepsilon - \varepsilon_2) v_2 f_2 = 0 \tag{3.61}$$

The theoretical problem that needs to be resolved for specific mixtures boils down to the determination of the field ratios f_2 or f_2 and f_1. Theoretically, the two formulations are equivalent but, when approximations have to be made for the values of the field ratios, this is no longer true. Most of the published mixture equations differ from one another in the approximations considered appropriate. As for which of the two formulations to use as a starting point, it would seem reasonable to use Equation 3.60 for the case of sparse inclusions in a continuous medium and Equation 3.61 when the volume fractions of the

two components are comparable. In the general case, the dielectric properties (in Equation 3.60 and Equation 3.61) are complex. However, under static or quasistatic conditions, the mixture equations hold for either permittivity or conductivity.

Maxwell (1891) was the first to characterize the field ratios for a system of sparse spherical inclusions in a homogenous medium under static field conditions and obtained:

$$\frac{\sigma - \sigma_1}{\sigma + 2\sigma_1} = \nu_2 \frac{\sigma_2 - \sigma_1}{\sigma_2 + 2\sigma_1} \tag{3.62}$$

where the subscripts 1 and 2 refer to the suspending medium and inclusions, respectively. In terms of permittivity, Equation 3.62 is known as the Rayleigh formula; in its complex form it is attributed to Wagner and commonly known as the Maxwell–Wagner equation. Other well-known mixture equations for spherical inclusions include:

Böttcher equation:

$$\frac{\varepsilon - \varepsilon_1}{3\varepsilon} = \nu_2 \frac{\varepsilon_2 - \varepsilon_1}{\varepsilon_2 + 2\varepsilon_1} \tag{3.63}$$

Bruggeman equation:

$$\left(\frac{\varepsilon - \varepsilon_1}{\varepsilon_2 - \varepsilon_1}\right)^3 + (1 - \nu_2)\frac{\varepsilon}{\varepsilon_1} = 1 \tag{3.64}$$

Looyenga equation:

$$\varepsilon^{1/3} = \nu_1 \varepsilon_1^{1/3} + \nu_2 \varepsilon_2^{1/3} \tag{3.65}$$

To first-order approximation, the above mixture equations revert to the same expression irrespective of the formulation of the problem and of the technique used to solve it. This is because the conditions of infinite dilution and the spherical shape enable an almost exact solution to the field ratio to be obtained.

Other formulations exist for different shape inclusions such as oblate and prolate spheroids. The subject has been reviewed by, among others, Van Beek (1967), Hanai (1968), Dukhin (1971), and more recently, Greffe and Grosse (1992), Sihvola and Lindell (1992), and Tinga (1992).

It is possible to extend mixture equations to multiple inclusions by using an iterative procedure (Tamasanis, 1992). For example, if $\varepsilon(\varepsilon_1, \varepsilon_2, \nu_2)$ is the effective permittivity of a binary mixture of background of permittivity ε_1, inclusion of permittivity ε_2, and volume fraction v_2, then a mixture with two types of inclusions identified with subscripts 2 and 3, respectively, can be described as a binary mixture of background permittivity $\varepsilon(\varepsilon_1, \varepsilon_2, v_2/1 - v_3)$ and inclusion of permittivity ε_3 and volume fraction v_3. The effective permittivity of such a mixture will be

$$\varepsilon(\varepsilon_1;\, \varepsilon_2,\, v_2;\, \varepsilon_3,\, v_3) \approx \varepsilon\left[\varepsilon\left(\varepsilon_1;\, \varepsilon_2,\, \frac{v_2}{1 - v_3}\right);\, \varepsilon_3,\, v_3\right] \tag{3.66}$$

The contributions of the different types of inclusion are added recursively in order of increasing density.

Where the assumptions used in their derivation can be approximated in the tissue model, mixture equations can be used to analyze the dielectric properties of biological materials in terms of their constituents. A few examples are given here to illustrate their application.

If the ionic conductivities of the suspending phase and that of a protein solution are known, say, by measurement at a frequency below the protein β dispersion, and if an assumption is made about the conductivity of the protein molecules, an appropriate mixture equation can then be used to determine the volume fraction of the inclusions, which, in this case, is the hydrated protein. In turn, this enables the amount of bound water to be calculated given that the fraction of anhydrous protein is known. Bull and Breese (1969) followed this approach and calculated the bound water for a variety of proteins. They evaluated the water fraction to be 0.6 g/g of protein. Pauly and Schwan (1966), following a similar procedure, estimated the conductivity of the human erythrocyte to be 0.518 S/m at 25°C, compared to the value of 1.45 S/m calculated from the known ionic composition of the cell. They attributed the difference partly to excluded volume by the protein-bound water and partly to decreased ionic mobility due to hydrodynamic effects.

Bound water in biological systems including tissue was estimated by applying mixture equations in the near-plateau region between the β and γ dispersions of the permittivity spectrum. Assuming the tissue to be a suspension of hydrated organic matter in an electrolyte solution that is little affected by the presence of the organic matter, the measured permittivity at 1 GHz is a reasonable estimate of the effective static permittivity. Knowledge of the permittivity of the suspending medium and an estimate of the permittivity of the organic matter enables the volume fraction of the inclusion to be calculated. Comparison with the known organic content provides an estimate of bound water (e.g., Grant et al., 1984; Kaatze, 1990; Schaefer et al., 2003).

3.6 Dielectric Relaxation Mechanisms in Heterogenous Media

The description of a material as heterogenous is a matter of scale; in the context of dielectric relaxation, it refers to electrical heterogeneity or the presence of electrical boundaries or interfaces. Boundary conditions at and around the interfaces gives rise to dielectric dispersions quite apart from dipolar-type dispersions that occur in the surrounding media. In biological materials, cellular membranes provide such interfaces; their presence is associated with two major dispersion regions in the dielectric spectra of tissues, namely, α and β dispersions originating mainly from interfacial polarization and ionic diffusion effects. The main mechanisms giving rise to these phenomena will be briefly discussed in this section.

3.6.1 Interfacial Polarization

Interfacial polarization is due to the charging of interfaces between conducting media and is an important mechanism of interaction in biological material. The basic principles of this phenomenon are best illustrated in simple models first before discussing their occurrence in biological materials.

3.6.1.1 Interface between Two Media

The simplest model is that of an interface between two media, for example, two slabs of thickness d_1 and d_2 in contact with each other with their interface perpendicular to an external electric field (Figure 3.14a). If the static permittivity and conductivity of the two materials are ε_1, σ_1 and ε_2, σ_2, respectively, the boundary condition on the electric field component normal to the interface gives

$$E_1\varepsilon_1 = E_2\varepsilon_2 \tag{3.67}$$

If the current densities j_1 and j_2 are equal, there will be no charge accumulation at the interface; this, however, is hardly ever the case. The ratio of current densities at the interface is

$$j_1/j_2 = \sigma_1 E_1/\sigma_2 E_2 = \sigma_1\varepsilon_2/\sigma_2\varepsilon_1 \tag{3.68}$$

Therefore, if $\sigma_1\,\varepsilon_2 \neq \sigma_1\,\varepsilon_2$, the interface will be charged at a rate that is proportional to the difference between j_1 and j_2.

The effective permittivity ε and conductivity σ of the system are calculated from its effective capacitance. With the field across the interface, this is equivalent to capacitances in series combination; thus,

$$\frac{d_1 + d_2}{\varepsilon - \mathrm{j}\sigma/\omega\varepsilon_0} = \frac{d_1}{\varepsilon_1 - \mathrm{j}\sigma_1/\omega\varepsilon_0} + \frac{d_2}{\varepsilon_2 - \mathrm{j}\sigma_2/\omega\varepsilon_0} \tag{3.69}$$

This can be rearranged into a Debye type expression with a relaxation time of

$$\tau = \varepsilon_0 \frac{\varepsilon_1 d_2 + \varepsilon_2 d_1}{\sigma_1 d_2 + \sigma_2 d_1} \tag{3.70}$$

and limiting values for low and high frequencies

$$\varepsilon_s = \frac{(\varepsilon_2\sigma_1 - \varepsilon_1\sigma_2)^2 (d_1 + d_2) d_1 d_2}{(\varepsilon_1 d_2 + \varepsilon_2 d_1)(\sigma_1 d_2 + \sigma_2 d_1)^2} + \varepsilon_\infty \tag{3.71}$$

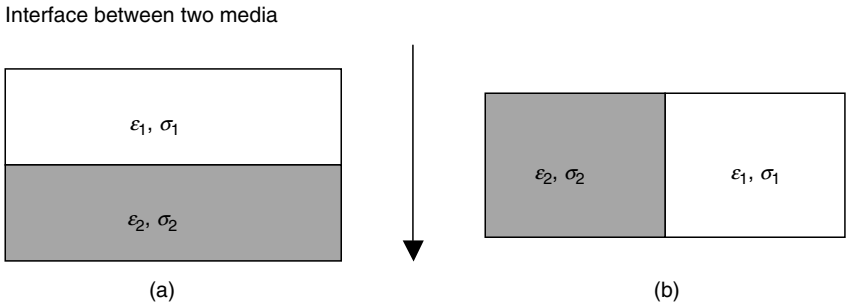

FIGURE 3.14
Two-media system; the arrow gives the direction of the electric field: (a) interface at right angle to the field and (b) interface along the field.

$$\sigma_s = (d_1 + d_2)\frac{\sigma_1\sigma_2}{\sigma_1 d_2 + \sigma_2 d_1} \tag{3.72}$$

$$\varepsilon_\infty = \frac{(d_1 + d_2)\varepsilon_1\varepsilon_1}{(\varepsilon_1 d_2 + \varepsilon_2 d_1)} \tag{3.73}$$

The polarization of the effective capacitance occurs in addition to any polarization process within the constituent phase, in which case the dielectric spectrum of the composite system will reflect the multiple dispersions.

If the field is along the interface (Figure 3.14b), no interfacial dispersion is observed, the effective permittivity is $\hat{\varepsilon} = (\hat{\varepsilon}_1 + \hat{\varepsilon}_2)/2$.

3.6.1.2 Suspension of Spheroids

The simplest system in this category is a dilute suspension of spherical inclusions in a continuum. Its effective complex permittivity is given by the formulation known as the Maxwell–Wagner equation, where the subscripts 1 and 2 refer to the suspending medium and inclusions, respectively:

$$\frac{\hat{\varepsilon} - \hat{\varepsilon}_1}{\hat{\varepsilon} + 2\hat{\varepsilon}_1} = v_2 \frac{\hat{\varepsilon}_2 - \hat{\varepsilon}_1}{\hat{\varepsilon}_2 + 2\hat{\varepsilon}_1} \tag{3.74}$$

This equation can be rearranged in the form of a dispersion equation with the following parameters:

$$\begin{aligned}
\varepsilon_\infty &= \varepsilon_2 \frac{2\varepsilon_2 + \varepsilon_1 - 2v_2(\varepsilon_2 - \varepsilon_1)}{2\varepsilon_2 + \varepsilon_1 + v_2(\varepsilon_2 - \varepsilon_1)} \\
\varepsilon_s - \varepsilon_\infty &= \frac{9(\varepsilon_2\sigma_1 - \varepsilon_1\sigma_2)^2 v_2(1 - v_2)}{[2\varepsilon_2 + \varepsilon_1 + v_2(\varepsilon_2 - \varepsilon_1)][2\sigma_2 + \sigma_2 + v_2(\sigma_2 - \sigma_1)]^2} \\
\sigma_s &= \sigma_2 \frac{2\sigma_s + \sigma_2 - 2v_2(\sigma_2 - \sigma_1)}{2\sigma_2 + \sigma_2 + v_2(\sigma_2 - \sigma_1)} \\
\sigma_s - \sigma_\infty &= \frac{9(\sigma_2\varepsilon_1 - \sigma_1\varepsilon_2)^2 v_2(1 - v_2)}{[2\sigma_2 + \sigma_1 + v_2(\sigma_2 - \sigma_1)][2\varepsilon_2 + \varepsilon_2 + v_2(\varepsilon_2 - \varepsilon_1)]^2} \\
\tau &= \varepsilon_0 \frac{2\varepsilon_2 + \varepsilon_1 - v_2(\varepsilon_2 - \varepsilon_1)}{2\sigma_2 + \sigma_2 + v_2(\sigma_2 - \sigma_1)}
\end{aligned} \tag{3.75}$$

The dispersion will occur when $\sigma_1\varepsilon_2 \neq \sigma_1\varepsilon_2$, which is practically always the case. The magnitude of the dispersion depends on the differences in dielectric parameters between the two phases.

In the context of mixture theory, sparse means $v_2 \leq 0.2$; to model the effective permittivity of more concentrated suspensions, it is necessary to take into consideration interparticle interactions. This becomes a very complex model; there are no rigorous solutions even for the relatively simple case of identical spherical inclusions. The Bruggeman–Hanai Equation 3.64 was formulated taking account of some interaction between particles and is therefore better suited than the Maxell–Wagner equation to model more concentrated suspension. In its complex form, it can be shown to predict the occurrence of a dispersion with the following limiting parameters:

$$\left(\frac{\varepsilon_\infty - \varepsilon_2}{\varepsilon_1 - \varepsilon_2}\right)\left(\frac{\varepsilon_1}{\varepsilon_s}\right)^{1/3} = 1 - v_2$$

$$\varepsilon_s\left(\frac{3}{\varepsilon_s - \sigma_2} - \frac{1}{\sigma_s}\right) = 3\left(\frac{\varepsilon_1 - \varepsilon_2}{\sigma_1 - \sigma_2} + \frac{\varepsilon_2}{\sigma_s - \sigma_2}\right) - \frac{\varepsilon_2}{\sigma_2}$$

$$\left(\frac{\varepsilon_s - \sigma_2}{\sigma_1 - \sigma_2}\right)\left(\frac{\sigma_1}{\sigma_s}\right)^{1/3} = 1 - v_2$$

$$\sigma_\infty\left(\frac{3}{\varepsilon_\infty - \varepsilon_2} - \frac{1}{\varepsilon_\infty}\right) = 3\left(\frac{\sigma_1 - \sigma_2}{\varepsilon_1 - \varepsilon_2} + \frac{\sigma_2}{\varepsilon_\infty - \varepsilon_2}\right) - \frac{\sigma_1}{\varepsilon_1} \tag{3.76}$$

In these expressions ε_s, ε_∞, σ_∞ are the limiting values of the corresponding parameters. The dispersion is characterized by a distribution of relaxation times.

The validity of the model has been verified experimentally for mixtures of known composition and geometry (Hanai et al., 1982; Ishikawa et al., 1982). The dispersion is broader than a single time constant because of the interactions between particles. Moreover, if the components of the heterogenous system exhibit molecular dielectric dispersion of their own, then these intrinsic dispersions will also appear, together with the interfacial dispersion, in the complete frequency spectrum of the system.

Fricke (1955), Sihvola and Kong (1988), Sihvola and Lindell (1992), and many others have extended the model to the more general case of a suspension of spheroids with any combination of axial ratios. Ultimately, the outcome is equivalent to introducing a parameter to account for the shape. The Maxwell–Wagner equation becomes

$$\frac{\hat{\varepsilon} - \hat{\varepsilon}_1}{\hat{\varepsilon} + F\hat{\varepsilon}_1} = v_2 \frac{\hat{\varepsilon}_2 - \hat{\varepsilon}_1}{\hat{\varepsilon}_2 + F\hat{\varepsilon}_1} \tag{3.77}$$

where F is the shape factor, equal to 2 for spheres, which reverts to Equation 3.74. In cases where the shape of the inclusion is not known, limiting values for the effective permittivity can be obtained using the shape factors in the extreme cases of infinitely long thin rods and infinitely thin circular disks.

An interesting case is that of ellipsoids with their axes aligned in the same direction. The permittivity would be different depending on the direction of the field; the mixture would be electrically anisotropic and the effective permittivity is represented by a tensor.

Another case of practical interest is that of layered spherical inclusions. This situation is required when modeling cellular structures surrounded by a membrane of finite thickness. Solutions for the effective permittivity of this model were provided by many researchers in this field (e.g., Schwan, 1957; Zhang et al., 1983; Grosse, 1988). These authors applied two mixture models, once to the concentric bodies, thus obtaining an effective permittivity for the inclusions, and then treating the mixture as a suspension of homogenous spheres. The parameters of the dispersion could be expressed in terms of the physical dimensions and electrical characteristics of the cell and cell membrane; simplified versions of these expressions are reported by Foster and Schwan (1989). Sihvola (1989) and Irimajiri et al. (1991), among others, extended the treatment to several concentric shells by using a recursive technique. These complex models are more relevant to the study of biological systems and to the understanding of the interactions at the cellular level. They are not sufficiently developed for the quantitative characterization of the interfacial polarization in biological systems, but do provide an insight into the factors that determine its characteristics. An example from the recent literature is the modeling of the dielectric response of heart tissue by Schaefer et al. (2002). The model is a function of the cell shape, electrical cell coupling and

polarization of cell membranes, and intracellular structure. It describes heart cells and subcellular organelles as rotational ellipsoids filled with electrolyte enclosed by an isolating membrane and is capable of reproducing the main features of the dielectric spectrum of heart tissue.

In recent years, statistical methods using probabilistic descriptions of the physical mixture in terms of a spatial density function have been developed to provide realistic bounds for the effective permittivity of mixtures. This approach, developed by, among others, Bergman (1978) and Milton (2002), provides an analytic integral representation of the effective permittivity $\hat{\boldsymbol{\varepsilon}}$ of an arbitrary binary mixture in terms of a spatial density function $g(x)$:

$$\frac{\hat{\boldsymbol{\varepsilon}} - \hat{\boldsymbol{\varepsilon}}_1}{\hat{\boldsymbol{\varepsilon}}_1} = \int_0^1 \frac{g(x)\,\mathrm{d}x}{x + \hat{\boldsymbol{\varepsilon}}_1/\hat{\boldsymbol{\varepsilon}}_2 - \hat{\boldsymbol{\varepsilon}}_1}$$

where, as before, the subscripts 1 and 2 refer to continuum and dispersed phases, respectively, and the integration is over all possible positions. Depending on the choice of distribution function $g(x)$, it is possible for the above equation to revert to some of the well-known binary mixture equations. Recursive application is possible; modeling biological systems remains challenging.

A new tool for the study of mixtures, including biological materials, has evolved with the development of increasingly powerful numerical modeling packages for the propagation of electromagnetic fields in complex structures from full solutions of Maxwell's equations. With structures being defined at the nanoscale, the characterization of fields within cells and subcellular structures appears to be within reach (Gimsa and Wachner, 1998, 1999, 2001a,b; Bianco et al., 2000; Sebastian et al., 2001; Munoz et al., 2003).

3.6.2 Counterion Polarization Effects

Another important polarization phenomenon in electrically biological materials originates from ionic diffusion effects near charged surfaces and the formation of counterion or electric double layers. The distribution of ions in the vicinity of charged interfaces is subject to concentration and electric field gradients; an equilibrium is reached with the ions continuously distributed over the volume of the electrolyte solution. The time constant associated with this mechanism is longer than that of the Maxwell–Wagner effect, it is of the form L^2/D, where L is the length over which diffusion occurs and D is a diffusion coefficient (Schwarz, 1962).

Counterion phenomena are difficult to analyze rigorously; they involve coupled electrodynamic and hydrodynamic mechanisms. The theories are complex, but good reviews are available as an introduction to the subject (Dukhin, 1971; Dukhin and Shilov, 1974; Fixman, 1980, 1983; Mandel and Odijk, 1984). Relatively simple models that provide exact solutions have been proposed (Grosse and Foster, 1987; Grosse, 1988), whereby coupled differential equations for the ion concentrations and current densities are obtained for a macroscopic sphere of radius a in an ionic medium. Their solution yields a broad, asymmetrical, low-frequency dispersion. The time constant of this dispersion is a^2/D, where D is the diffusion coefficient of ions in the bulk electrolyte.

To visualize the effect, consider the motion of an ion in the bulk electrolyte near the particle, it will be conducted away or excluded depending on whether its sign is the same or opposite that of the ions in the counterion layer. Thus, for an ion in the electrolyte, the particle acts either as a good conductor or as an insulator depending on its charge

compared to that of the counterion. A cloud of charge accumulates within a Debye length of the charged surface; for physiological saline (0.15 N NaCl) the Debye length is very small, <1 nm, resulting in a very large induced capacitance and hence a large permittivity dispersion.

3.7 Dielectric Properties of Tissue—State-of-Knowledge

Research into the dielectric properties of biological materials and their variation with frequency has been ongoing for most of the past century. Early studies went a long way toward understanding and establishing the principles of interaction and the corresponding features of the highly frequency-dependent spectrum of a tissue. In the last few decades, the research was driven, above all, by the need to establish a credible database of dielectric properties of all body tissues for use in electromagnetic dosimetry studies, where the object is to quantify the exposure of people to external electromagnetic fields from knowledge of the effective internal fields and currents induced in them. In these studies, tissues are characterized by their measured dielectric properties. In the last decade, most dosimetric studies drew on data published in the scientific literature in 1996 and made widely available on the Internet thereafter (Gabriel et al., 1996; Gabriel and Gabriel, 1997).

3.7.1 1996 Database

The backbone of the 1996 database is a large experimental study providing data pertaining, almost exclusively, to excised animal tissue at 37°C. For most tissues, the characterization was over a wide frequency range, 10 Hz to 20 GHz, using three previously established experimental setups with overlapping frequency ranges. The following are some of its characteristics:

- The data are presented in the context of a review covering all relevant publications in the preceding half-century. By and large, the experimental data were well within the confines of corresponding values from the literature.
- The data showed good internal consistency, that is, good agreement between data obtained with different experimental setups in a common frequency range.
- Finally, an element of great practical importance, the dielectric spectra were parametrized using a multidispersion model consisting of four Cole–Cole terms and one ionic conductivity term. For each tissue, the parameters of the model enable the reconstruction of its spectrum, a procedure that could easily be incorporated in numerical studies to provide dielectric data that are broadly in line with the vast body of literature on the subject.
- The fact that the complex permittivity data could be fitted to Cole–Cole dispersions implies that they also agree with the Kramers–Kronig relation in accordance with the principle of causality for a linear system. This imparts another level of consistency to the data.

Examples are given here to illustrate the extent of the available data in the literature for certain tissues at certain frequencies in contrast to the scarcity of data elsewhere

(Figure 3.15 through Figure 3.17). No attempt is made at a quantitative or mechanistic analysis.

While useful, the 1996 database has several limitations, as pointed out by its authors:

- Most measurements were carried out on excised tissue, while data pertaining to live tissue would have been more relevant in bioelectromagnetics studies.
- For most tissues, the predictions of the model can be used with confidence for frequencies above 1 MHz because of the availability of supporting data in the literature.
- At lower frequencies, where the literature values are scarce and have larger than average uncertainties, the model should be used with caution in the knowledge that it provides a ''best estimate'' based on the then available knowledge. This is particularly important for tissues where there are no data to support its predictions.
- Electrode polarization, an inevitable source of error at low-frequencies, was not totally accounted for. It affects the data at frequencies below 100 Hz.
- Because of the geometry of the sampling probe, it was not possible to orient the field along and across directed structure to demonstrate the anisotropy of the dielectric properties.

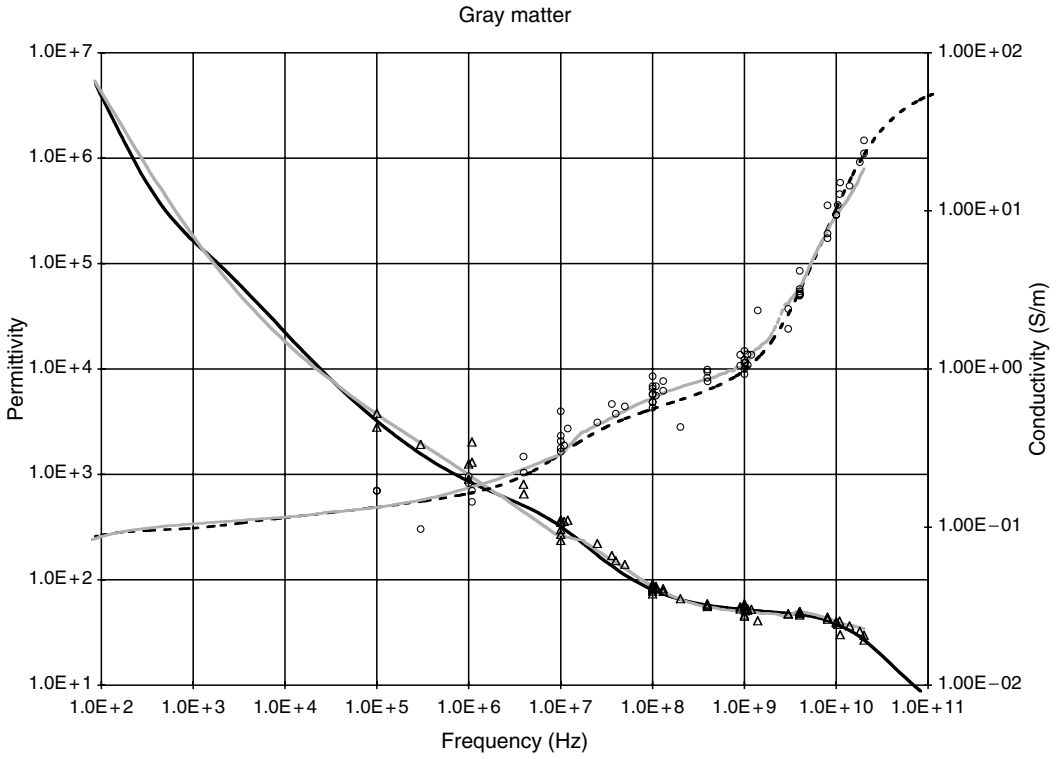

FIGURE 3.15
Permittivity and conductivity of gray matter at 37°C; gray lines are experimental data from Gabriel et al. (1996), triangles and circles are permittivity and conductivity values from the pre-1996 literature, black solid and dashed lines are the predictions of the model.

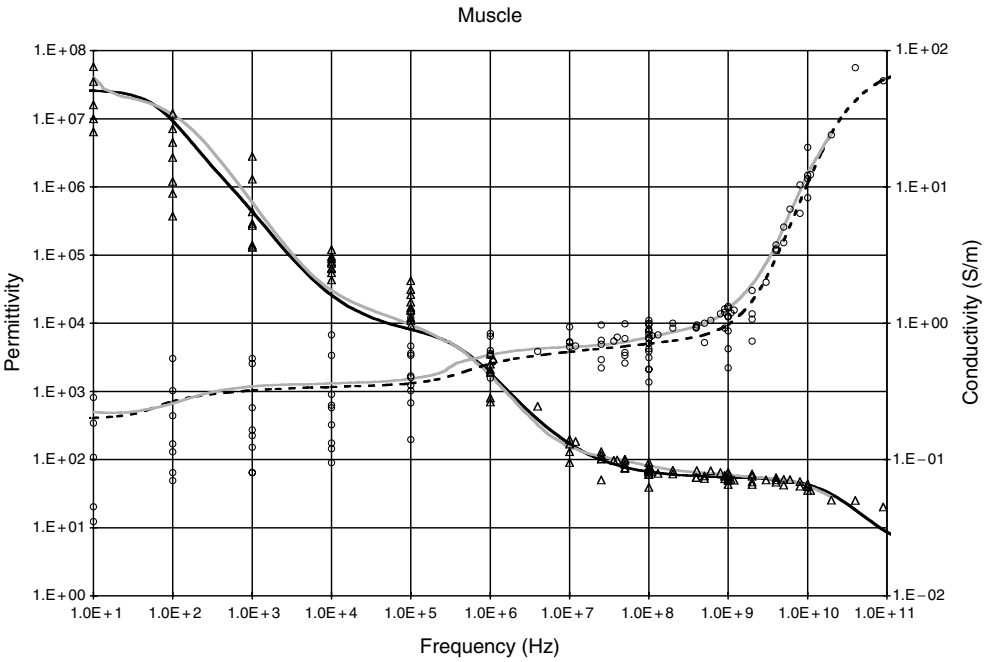

FIGURE 3.16
Permittivity and conductivity of skeletal muscle at 37°C; legend as in Figure 3.15. The very wide spectrum of data below 1 MHz is, at least partially, due to the anisotropy in the dielectric properties of muscle tissue. The literature data pertain to measurement along and across the muscle fibers and to measurements where the direction was not specified.

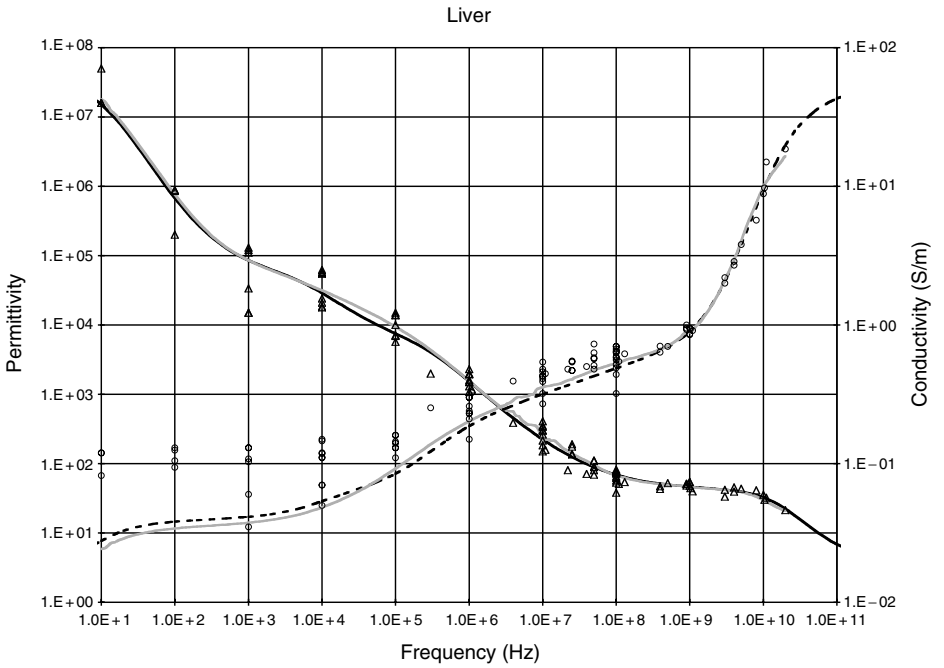

FIGURE 3.17
Permittivity and conductivity of liver tissue at 37°C; legend as in Figure 3.15. Liver tissue exhibits no significant anisotropy in its dielectric properties, but as with all tissue, the characteristics of the β dispersion and the static conductivity are sensitive to the viability and time after death when the measurements were made.

Evidently, much remains to be done, in particular with respect to reducing the uncertainty in the data and filling in the gaps identified. Ten years on, the recent literature is reviewed to update the state-of-knowledge on the subject.

3.7.2 Literature After 1996—A Brief Review

The review is carried out per tissue type or thematic underline. In some cases, data from recent studies are compared with the model in the 1996 database and with data from a recent study, where the dielectric properties of over 40 tissues were characterized *in vivo* and *in vitro* in the frequency range 10^2 to 10^4 MHz (Peyman et al., 2005).

3.7.2.1 Brain Tissue: Gray and White Matter

At microwave frequencies, three studies reported new data for brain tissue (Bao et al., 1997; Schmid et al., 2003a,b). Data tabulated by the authors are given in Figure 3.18. Data by Peyman et al. (2005) are in reasonable agreement with the database, while data by Bao and coworkers and Schmid and coworkers are higher for both permittivity and conductivity.

It is important to find a reason as to why carefully conducted studies, using adaptations of a conceptually similar experimental procedure, are still coming up with different results. In terms of explanation we note the handling of the sample by Bao et al., in which the whole brain is excised, immersed in saline, temperature regulated, and measured while immersed. The authors give good reasons for following this procedure.

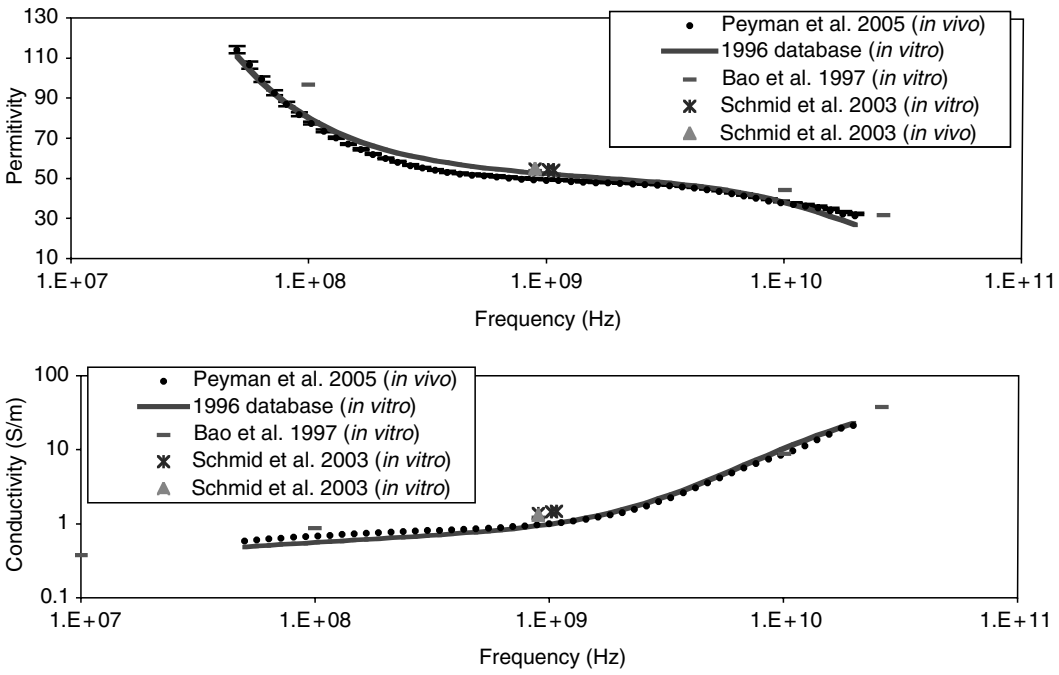

FIGURE 3.18
Dielectric properties of gray matter at 37°C. Data from recent studies compared to the prediction of the 1996 database.

It is inevitable, however, that one should expect their data to fall on the high side of average because of the presence of saline. Schmid et al. published data on porcine (*in vivo*) and human gray matter (*in vitro*). Their porcine gray matter data were obtained under conditions designed for the study of variation with time over a period spanning the time of death and beyond. Presumably, this is why their measurements were carried out over a narrow frequency range with the measurement probe held in position for the duration of the experiment (150 min). One might speculate that the amount of pressure used to maintain constant contact between the probe and the live brain could cause local oozing of fluid and higher conductivity values.

Conjecture apart, these data are valuable additions to the literature, but one must be cautious not to generalize on the basis of such limited data that measurement *in vitro* underestimates the dielectric properties of living tissues at microwave frequencies. Differences between tissue properties obtained *in vivo* and *in vitro* are to be expected at lower frequencies, in the range of α and β dispersions, in view of the sensitivity of their causal mechanism to the physiological state of the tissue. Differences between *in vivo* and *in vitro* data are much less likely in the frequency range of the γ dispersion, where water content is the most important determinant factor, and as recently reported by Stauffer et al. (2003), for liver tissue, and by Peyman et al. (2005), for many tissues including gray matter. Measurements *in vivo* are fraught with difficulties. For example, Burdette et al. (1986) measured the gray matter, *in vivo*, through the pia matter and directly beneath it. Of the two sets of data obtained, one is similar to that of Schmid et al., and the other is significantly lower.

In their human study, Schmid et al. measured the dielectric properties of gray matter in the frequency range of 800 MHz to 2450 MHz on 20 human brains immediately after excision. The measurements were carried out at room temperature in the range 18°C to 25°C and extrapolated to 37°C using experimentally determined thermal coefficients. Nevertheless, the dielectric properties at 900 MHz were in very good agreement with their data for porcine gray matter *in vivo*. It is understandably frustrating to realize that the bounds of uncertainty remain high when comparing data from different laboratories, even for those tissues that have been widely measured and reported.

Latikka et al. (2001) reported conductivity values at 50 kHz for gray matter (0.28 S/m), white matter (0.25 S/m), cerebrospinal fluid (1.25 S/m), and tumors (0.1 S/m to 0.43 S/m). They used a monopolar needle electrode during brain surgery on nine patients who had deep brain tumors. The technique is not geared toward making directed measurement and detecting anisotropy in the electrical properties, although those are anticipated on theoretical grounds and are known to be present in the hertz to kilohertz frequency range (Nicholson, 1965; Ranck et al., 1965; Yeldin et al., 1974; Nicholson and Freeman, 1975). Observed differences in the conductivity along and across the cellular structure were factors between 2 and 10 depending on the tissue. Clearly, this is an area of importance to electrophysiology, among other applications; it is also an area where data are scarce.

Peyman et al. (2001) reported variation in the dielectric properties of rat brain tissue as a function of age, at microwave frequencies. Their data pertained to the whole brain. The observed variation was ascribed, at least partially, to the change in the ratio of gray to white matter, which is known to occur throughout the developmental stage. In a recent study on porcine tissues (Peyman et al., 2005), they were able investigate gray and white matter separately. In this case, no variations were observed in the dielectric spectrum of gray matter, while statistically significant variations were observed in the dielectric spectrum of white matter (Figure 3.19). The observed variations are probably related to the process of myelination, which begins at birth and lasts to maturation. Similar variations were observed in the dielectric properties of the spinal cord.

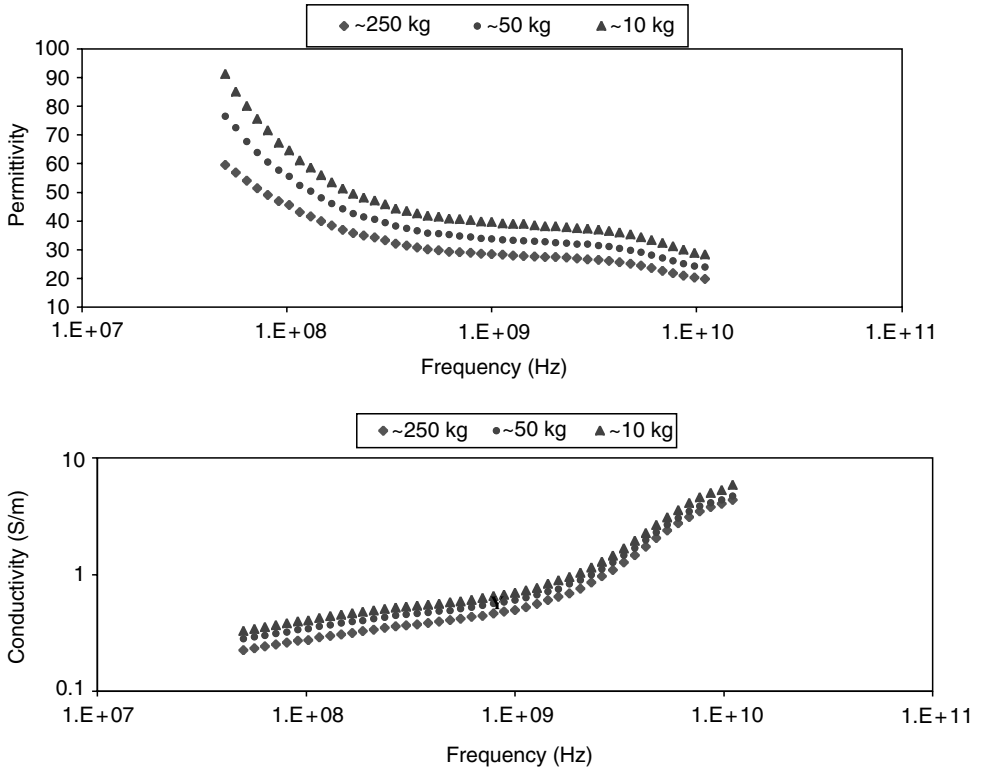

FIGURE 3.19
Permittivity and conductivity of white matter as a function of animal growth. The measurements were made *in vitro* at 37°C. The lowest permittivity and conductivity spectra pertain to a fully grown, 250-kg sow, the highest to a 10-kg piglet. (Data are from Peyman A, Holden S, Gabriel C. 2005. Dielectric Properties of Biological Tissues at Microwave Frequencies. Final technical report, MTHR Department of Health, U.K.)

3.7.2.2 Liver

Dielectric data for liver tissue were reported in several studies carried out under different conditions for a variety of reasons. For example, Riedel et al. (2003) developed a contact-free inductive measurement procedure and demonstrated the system by carrying out conductivity measurements on liver tissue between 50 and 400 kHz as a function of time after death. Stauffer et al. (2003) characterized the dielectric properties of normal and cancerous liver tissue in the frequency range of 0.3 to 3 GHz and reported higher permittivity and conductivity for tumor tissue. Chin and Sherar (2001) observed irreversible changes in the dielectric properties of liver tissue at 915 MHz because of excessive heating causing protein denaturation. Haemmerich et al. (2002) reported changes in the electrical resistivity of liver tissue during induced ischemia and postmortem. They observed increases in resistivity *in vivo* during occlusion. They analyzed the data in terms of intra- and extracellular resistance and cell membrane capacitance.

Valuable contributions by Raicu et al. (1998a,b) have provided data for rat liver tissue, measured *in vivo*, in the frequency range of 10^2 to 10^8 Hz. This is an eventful part of the dielectric spectrum of a tissue where contributions from interfacial and counterion interaction mechanisms occur. The measured data were corrected for electrode polarization and found to be in reasonable agreement with some previous studies (Surowiec et al., 1986; Foster and Schwan, 1996; Gabriel et al., 1996c). As expected, the data obtained traced a broad dielectric dispersion curve over the range of 10^3 to 10^8 Hz, suggestive of the

involvement of widely distributed relaxation times. In the second of their 1998 papers, they provide a mechanistic analysis. A simple application of the Maxwell–Wagner interfacial polarization theory could not fully explain the observed dielectric behavior, especially at frequencies below 1 MHz. The Bruggeman–Hanai-type effective medium theory (EMT) was better, but not perfect, at simulating the observation at low-frequencies. A better simulation of the effective permittivity was obtained when second-order corrections, for possible dipole–dipole interaction (DDI) effects, were introduced to the classical EMT for a concentrated suspension of particles. Application of the new EMT-DDI model enabled reasonable estimates to be made of the following: effective size and shape of hepatic cell; specific capacitance for the plasma, nuclear, and mitochondrial membranes associated with the hepatocyte; and cytosolic as well as nucleoplasmic conductivities of physiological interest.

3.7.2.3 Muscle

Muscle tissues, be it skeletal, myocardial, lingual, or other, exhibit large anisotropy in their electrical properties. This is to be expected from the tissue structure and was observed at frequencies below 1 MHz (Epstein and Foster, 1983; Fallert et al., 1993). The static conductivity value measured along the muscle fiber may be up to an order of magnitude higher than when measured across. The α dispersion is more prominent and the β dispersion less defined in the longitudinal direction in accordance with the predictions of effective permittivity modeling of elongated structures. For example, Semenov et al. (2002) evaluated anisotropy of the myocardium using a cellular model of the myocardial tissue and concluded that at frequencies lower than 10 MHz, myocardial dielectric properties are highly anisotropic (up to a factor of 10). Reliable, low-frequency data are very scarce, and there is a wide range in what is available in the literature, partly due to the fact that many authors do not specify the measurement orientation. The situation is not helped by the fact that the apparent anisotropy depends on the measurement procedure, in particular the interelectrode distance in relation to the size of the muscle fiber. Some of the problems associated with obtaining good data at frequencies below 1 MHz have been described by Tsai et al. (2000, 2002) in the context of their *in vivo* measurement of swine myocardial resistivity. In their study, they report changes in the myocardial resistivity as a function of time after death. The postmortem resistivity at 1, 10, and 100 Hz increased to about three times their original *in vivo* value and at 500 kHz and 1 MHz increased less than 15%, 6 h after death.

Most recent studies on the electrical properties of muscle tissue focused on the differences between normal and ischemic or hypoxic tissue. One of the drivers is to investigate the possibility of using *in situ* impedance measurements to map the histological changes in tissue *in vivo*. There is also potential for noninvasive imaging provided that the electrical characteristics of both normal and scar tissue are well-defined. Miyauchi et al. (1999) and Schaefer et al. (1999) observed changes in the α and β dispersions of normal and ischemic skeletal muscle. Ischemia in myocardial muscle is a matter of clinical importance in the assessment of myocardial infarction and has been the subject of many dielectric investigations. Schwartzman et al. (1999) investigated the properties of the border zone, which were found to be intermediate between healthy and infarcted tissue in the case of chronically infarcted ventricular myocardium. Semenov et al. (2002) observed the dielectric properties of canine myocardium during acute ischemia and hypoxia to explore the potential of these observations for the clinical assessment of myocardial tissue using electrical impedance and microwave tomography. One of the problems identified is the need to know and take into consideration the tissue electrical anisotropy.

3.7.2.4 *Skin*

Skin is the interface of the body with environmental agents including electromagnetic fields; knowledge of its dielectric properties is of importance in the assessment of human exposure and in numerous biomedical applications. Data from *in vivo* measurements are now available, obtained using noninvasive, open-ended coaxial probes (Gabriel et al., 1996c; Gabriel, 1997; Raicu et al., 2000). However, the interpretation of such topical measurements as effective permittivity of the skin is far from straightforward. Lahtinen et al. (1997) and Alanen et al. (1998) advocate an analysis based on a quasistatic approximation of the fringing field of the probe penetrating a layered structure. Gabriel (1997) drew attention to the effect on the dielectric spectrum of the degree of hydration of the stratum corneum (Figure 3.20), which also affects penetration of the field into the tissue. Joining the discussion, Raicu et al. (2000) carried out *in vivo* measurements on dry skin and on skin moistened with physiological saline, in the frequency range of 100 Hz to 100 MHz. They analyzed the data using the dispersion model comprising a Debye-type and ''universal'' responses (Equation 3.53) and a conductivity term. Comparing the parameters of the model for dry and saline-moistened skin, they noted a fivefold increase in the dispersion magnitude. One possible explanation they provide is that the ''effective penetration depth'' increases and contributions from the innermost skin layers become evident. This statement appears paradoxical; in fact, it is due to the reduction in the layering effect; when moistened, the skin appears more homogenous and behaves like a high water content tissue.

Raicu et al. (2000) further speculate that an interfacial polarization originating from the stratum corneum–epidermis interface occurs in the case of dry skin, as suggested by Alanen et al. (1999), but not in that of the saline-moistened skin. In support of this argument, they refer to the change in one of the distribution parameters, β, which decreases from 0.152 to 0.076 after the skin is hydrated with aqueous NaCl solution. It therefore appears that topical measurement on dry (normal) skin *in vivo* may not be proportionately representative of the inner layers. On the other hand, the use of an aqueous coupling agent that is likely to hydrate the stratum corneum affects the results of the measurements. In practice, the use of a coupling agent gives more reproducible results and leads to better agreement between data from the recent literature, as is evident in Figure 3.21 through Figure 3.23, which contain such data (Gabriel, 1997; Ghodgaonkar et al., 2000; Raicu et al., 2000; Sunaga et al., 2002; Hwang et al., 2003; Petaja et al., 2003) and collectively cover the frequency range of 100 Hz to 100 GHz.

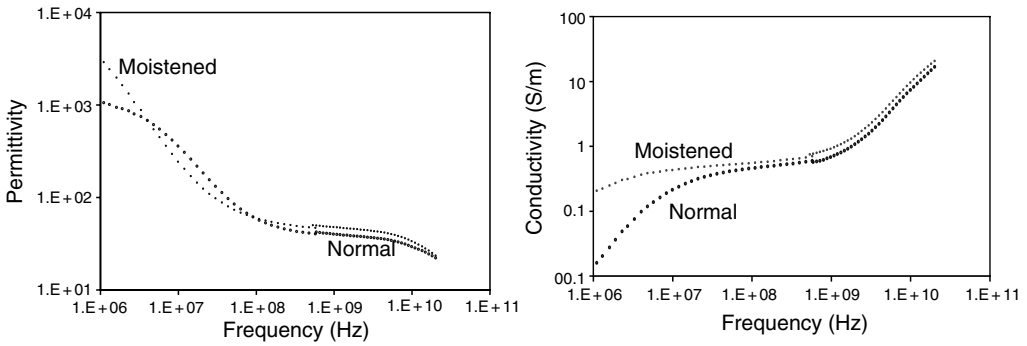

FIGURE 3.20
Permittivity and conductivity of skin (ventral forearm) illustrating the effect of moistening the skin on the dielectric spectra (Gabriel, 1996).

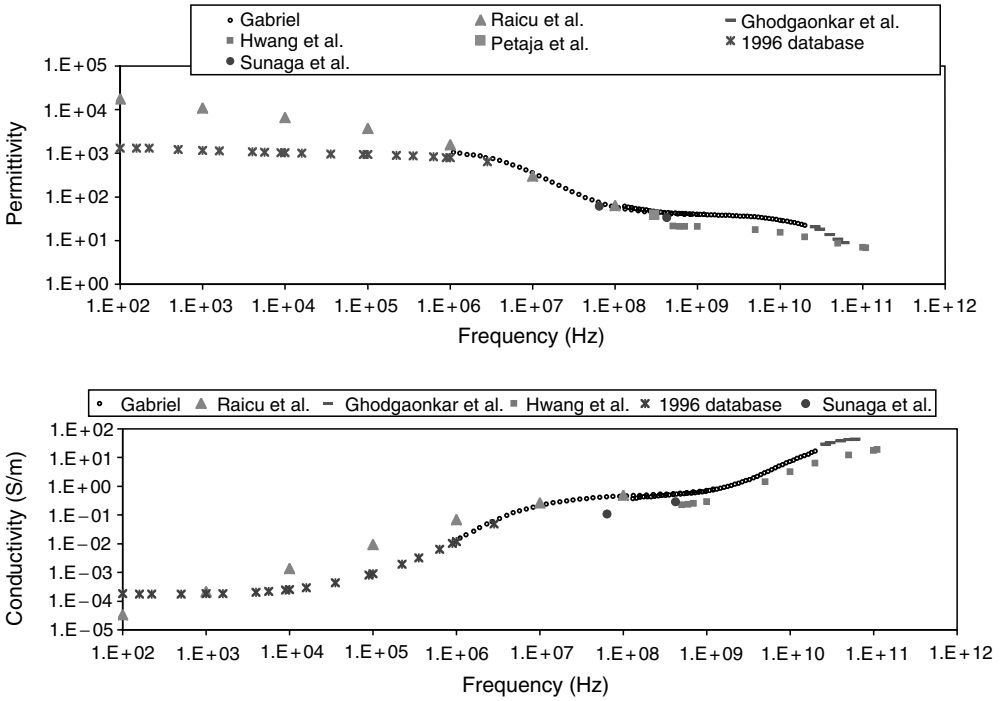

FIGURE 3.21
Permittivity and conductivity of skin (different parts of the body, excluding palms and soles). No moistening or contact gel was used. Different measurement techniques were used including open-ended coaxial probes of vastly different sizes.

The dielectric properties of skin have been widely investigated as monitors of various pathological conditions. Hayashi et al. (2005) investigated the dielectric properties of human skin *in vivo* at frequencies up to 10 GHz to monitor the progress of the healing process of skin burns using water content as the determinant factor. Their measurement technique, time domain spectroscopy and open-ended probe, is similar to that used by

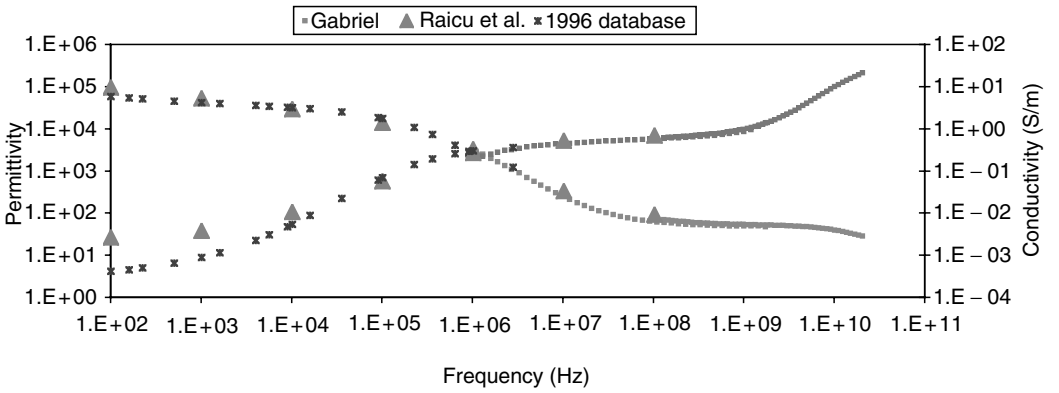

FIGURE 3.22
Permittivity and conductivity of skin (Raicu et al.: back of neck, moistened with physiological saline; Gabriel and database: ventral forearm, moistened with water). Open-ended coaxial probes of vastly different sizes were used.

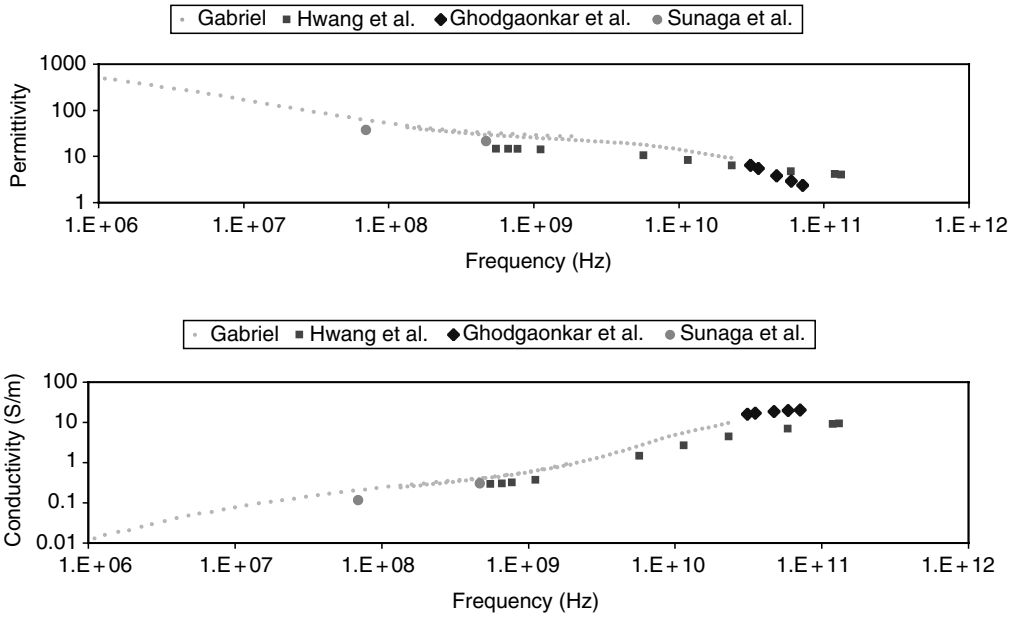

FIGURE 3.23
Permittivity and conductivity of palm, from recent studies.

Gabriel et al. (1997), who reported the dielectric spectra of normal and wounded tissue and ascribed the differences to water content.

Petaja et al. (2003) attempted to correlate the dielectric properties of skin at 300 MHz to body fluid changes after cardiac surgery and report limited success. Sunaga et al. (2002) investigated the variability in the dielectric properties of human skin of healthy volunteers, collagen disease patients, and dialysis patients over the frequency range of 1 to 450 MHz. No significant difference was detected in the dielectric properties among the three groups; some regional (abdomen, thigh, and forearm) dependence was observed. Marzec et al. (1999) measured the conductance and susceptance of soles and calves in leg skin from healthy controls and patients with ischemia in the frequency range of 100 Hz to 100 kHz. Ischemia was found to have no effect on the admittance at frequencies lower than 10 kHz, where the effect of the stratum corneum is dominant. Observed differences at frequencies in excess of 10 kHz are ascribed to ischemia in the underlying skin tissue.

Lindholm-Sethson et al. (1998) investigated the potential of using noninvasive skin impedance spectroscopy for the early detection of diabetic changes. They implemented a multivariate data analysis procedure to demonstrate how a regression model between the skin impedance and other diagnostic data for diabetic and control groups can be developed into a novel diagnostic tool for the early discovery of possible complications in diabetic patients. Statistical procedures are increasingly being applied to correlate dielectric parameters to structural or compositional elements of biological material, particularly in cases where there is a physical mechanism underpinning the effect that is obscured by noisy data (Kent et al., 2002).

The use of dielectric spectroscopy to monitor damage to the skin caused by ionizing radiation is an active field of research aiming at monitoring the side effects of clinical radiotherapy objectively and quantitatively. It appears that the changes to the skin during

the acute stage cause both permittivity and conductivity to decrease (Tamura et al., 1994; Nuutinen et al., 1998), while the reverse happens when radiation-induced fibrosis finally sets in (Lahtinen et al., 1999). The initial decrease in permittivity, which also means a decrease in skin water, may be due to damage to skin capillaries resulting in swelling of the cytoplasm, with narrowing or occlusion of capillaries and a reduction in the effective microcirculation of the skin. In the long term, an increase in collagen and collagen-bound water is a likely explanation for the observed increase in the permittivity in line with a clinical indicator of subcutaneous fibrosis (Nuntineu, 1998).

3.7.2.5 Bone

Peyman et al. (2001) observed variation in the dielectric properties of rat skull bone as a function of developmental stage from neonate to 70 days old. They reported lower permittivity and conductivity values across the spectrum (100 MHz to 20 GHz). Similar results were recently reported for porcine skull, cortical bone, and bone marrow (Peyman et al., 2005).

3.7.2.6 Dielectric Properties of Cancerous Tissue

The pathological differences between normal and cancerous cells affect their composition and morphology and shape their dielectric spectrum. Interest in this field of study is driven by biomedical applications where such differences can be exploited for the treatment or diagnosis of cancer. Most of the clinical applications are based on hyperthermia, whereby electromagnetic energy is preferentially applied to the cancerous tissue, usually as an adjunct to radiotherapy. Electromagnetic hyperthermia was an active field of study in the 1980s, and it remains the domain of specialist medical centers. In contrast, there is a growing interest in applications geared toward the detection of cancerous regions using three-dimensional microwave tomography procedures and signal analysis (Hagness et al., 1998, 1999; Bulyshev et al., 2001; Wersebe et al., 2002). In cases where the suspect region is accessible for dielectric measurements, the procedure relies on the characterization and comparative analysis of the dielectric spectrum (Walker et al., 2000). The ultimate goal is to detect changes at the precancerous stage prior to their visibility by x-rays and to the emergence of serious clinical symptoms.

There is evidence that tumors have higher water content than the corresponding normal tissue; for certain types of tumor, such as breast carcinoma surrounded by fatty tissue, the difference could be considerable. In terms of dielectric properties, one would expect cancerous tissue to have higher permittivity and conductivity at microwave frequencies compared to normal tissue, as observed and reported by Schepps and Foster (1980), Foster and Schepps (1981), Rogers et al. (1983), and more recently, Stauffer et al. (2003).

Morphological changes affect the dielectric properties in the frequency range of the β dispersion and can be quite significant (Smith et al., 1986). Walker et al. (2000) used a finite element analysis to model the differences in impedivity between normal and precancerous cervical cells in the frequency range of 100 Hz to 10 MHz. Their results showed significant differences at frequencies lower than 10 kHz, basically in line with measurements carried out *in situ* with a four-electrode pencil probe. Polevaya et al. (1999) used time domain dielectric spectroscopy to study the differences between normal and malignant white blood cells. They used a Maxwell–Wagner mixture formulation and a double-shell cell model to determine differences in cellular and nuclear membrane characteristics between normal and malignant cells. Their detailed analysis reflects on some functional differences between membranes and provides some insight into the etiology of cancer.

The use of the electrical characteristics of tissue to understand, image, or treat cancerous tissue relies on the availability of good representative data across the spectrum but particularly in the frequency range of the β dispersion, where the changes are specific to the cellular transformation as well as the water content.

3.7.2.7 Conductivity of Tissue at Low-Frequency

There are limited, reliable dielectric data for body tissue at frequencies below 100 kHz. Some of the reasons relate to the dependence of the dielectric properties on the physiological state, degree of perfusion, time after death, and other biological parameters. There are also experimental difficulties, in particular electrode polarization, which is a major source of systematic error at frequencies below 100 Hz, even when precautions are taken to minimize its effects. Based on typical tissue dielectric data and a simple model for the electrode polarization, it is possible to estimate that it affects the permittivity more than the conductivity and that for body tissue, the conductive rather than the capacitive component dominates its electrical admittance (Schwan, 1992). For this reason, at extremely low-frequencies, the conductivity of tissue is considered real rather than complex, and the body is modeled as a resistive network the parameters of which are determined by the conductivity of the various tissues.

The conductivity of body tissue can be estimated by modeling on a cellular scale and applying appropriate mixture equations. Using this approach, Peters et al. (2001) evaluated the effective conductivity of several tissues such as cerebral cortex, liver, and blood. Such studies help to place upper and lower bounds on the conductivity values based on cellular parameters and knowledge of the conductivity of the phases.

Faes et al. (1999) carried out a meta-analysis of review studies (Geddes and Baker, 1967; Stuchly and Stuchly, 1980; Duck, 1990; Gabriel et al., 1996a,b) of tissue conductivity in the frequency range 100 Hz to 10 MHz. To make relative comparisons between different tissues, they calculated the mean and 95% confidence interval. They found large confidence intervals such that the conductivities of most high water content tissues (skeletal and cardiac muscle, kidney, liver, lung, and spleen) were not statistically different from one another at that level of significance. In contrast, blood has higher conductivity, while bone and fat have demonstrably lower conductivities. The insignificance of differences in high water content tissues could, of course, imply an equality of their conductivities, but it could also point at a large source of experimental variation that obscures real differences.

The conductivity of the body, or body parts, can be obtained by volume averaging using anatomical models and individual tissue conductivity as in Table 3.4, where the conductivity of the whole and the various parts of the body is given based on tissue conductivity in Gabriel (2000) and a voxel anatomical human model (Dimbylow, 1996).

At 50 Hz, the calculated conductivity values are comparable to the commonly used estimate of 0.2 S/m for the effective permittivity of a homogenous body model. When dielectric data become available, it would become imperative to reexamine the whole

TABLE 3.4

Conductivity (in S/m) of the Whole and Parts of the Body Obtained by Volume Averaging

Frequency	Whole Body	Head	Torso	Arm	Leg	Neck
50 Hz	0.22	0.25	0.22	0.19	0.20	—
10 kHz	0.28	0.28	0.26	—	0.24	0.22
100 kHz	0.29	0.30	0.33	—	0.24	0.24

Source: From Gabriel (2000).

question of whether or not there is sufficient justification for neglecting the contribution of the capacitive element of the body's electrical properties.

3.7.2.8 Nonlinear Dielectric Properties

The polarization mechanisms discussed so far occur from interactions with weak fields eliciting linear responses. At high field strength, nonlinear molecular and cellular polarization phenomena are predicted on theoretical grounds, on the basis of induced dipolar properties and classical electrodynamics. The threshold for initiating such effects is system and frequency dependent. As a general rule, as the frequency increases, so does the field level required to cause an effect. In general, at frequencies below the manifestation of the β dispersion, field strengths of the order of 10^6 V/m may be capable of initiating polarization mechanisms that affect the cellular function; higher fields may cause dielectric breakdown within the membrane, ultimately leading to cell destruction.

Under controlled conditions, high field strength, nonlinear effects are the focus of numerous applications in biotechnology. For example, dielectrophoresis, or the motion of particles caused by electrical polarization effects in nonuniform fields, is used to separate and manipulate cells. For a review of this subject, see Pethig (1996). Another nonlinear phenomenon, electroporation, is a consequence of the electrical breakdown of biological membranes, resulting in the formation of pores and a significant increase in the membrane permeability to external ions and molecules. Under controlled conditions, electroporation could be reversible and used to advantage in therapeutic, drug delivery applications. The basic principles can be found in mechanistic studies by Plickett and Weaver (1996), Prausnitz et al. (1999), and many others.

The hypothesis that weak fields may trigger nonlinear effects in cells has been investigated in theory and practice (Weaver and Astumian, 1990; Woodward and Kell, 1990). The generation of harmonics is one aspect that can be used to monitor their occurrence (Woodward and Kell, 1990); it also means that the dielectric properties are nonlinear, responding to harmonics as well as to the fundamental frequency. The study of harmonics is a subtle and clever tool; it has yet to prove its effectiveness in monitoring physiological responses to weak fields.

More recently, Balzano (2002) proposed to use a similar approach to test whether biological cells exhibit nonlinear responses to weak fields, at microwave frequencies. His idea hinges on the possibility of detecting a microwave signal at 1.8 GHz (second harmonic of 900 MHz) as weak as one microwave photon per cell per second. An experimental project based on this hypothesis is currently under way (see MTHR Web site: http://www.mthr.org.uk/research_projects/HO_funded_projects_excell.htm, accessed August 5, 2005). It will help to clarify the issue of nonlinear dielectric properties.

References

Alanen E, Lahtinen T, Nuutinen J. 1998. Variational formulation of open-ended coaxial line in contact with layered biological medium. *IEEE Trans Biomed Eng* 45(10): 1241–1248.

Alanen E, Lahtinen T, Nuutinen J. 1999. Penetration of electromagnetic fields of an open-ended coaxial probe between 1 MHz and 1 GHz in dielectric skin measurements. *Phys Med Biol* 44: N169–N176.

Balzano Q. 2002. Proposed test for detecting nonlinear responses in biological preparations exposed to RF energy. *Bioelectromagnetics* 23(4): 278–287.
Bao JZ, Lu ST, Hurt WD. 1997. Complex dielectric measurements and analysis of brain tissues in the radio and microwave frequencies. *IEEE Trans Microwave Theory Tech MTT* 45(10): 1730–1741.
Barthel J, Buchner R, Munsterer M. 1995. The dielectric properties of water in aqueous electrolyte solutions. In: *Chemistry Data Series 12*, Kreysa G, Ed., DECHEMA, Frankfurt.
Bateman JB, Gabriel C. 1987. Dielectric properties of aqueous glycerol and a model relating these to the properties of water. *J Chem Soc Faraday Trans* 2(83): 355–369.
Bateman JB, Gabriel C, Grant EH. 1990. Permittivity at 70 GHz of water in aqueous solutions of some amino acids and related compounds. *J Chem Soc Faraday Trans* 2(86): 3577–3583.
Bateman JB, Evans GF, Brown PR, Gabriel C, Grant EH. 1992. Dielectric properties of the system bovine albumin: urea: betaine in aqueous solutions. *Phys Med Biol* 37: 175.
Bergman DJ. 1978. The dielectric constant of a composite material. *Phys Rep* C43: 377.
Bianco B, Giordano S. 2003. Electrical characterization of linear and nonlinear random networks and mixtures. *Int J Circ Theor Appl* 31: 199–218.
Bianco B, Chiabrera A, Giordano S. 2000. DC-ELF characterization of random mixtures of piecewise nonlinear media. *Bioelectromagnetics* 21: 145–149.
Böttcher CJF, Bordewijk P. 1978. *Theory of Electric Polarization*. Elsevier, Amsterdam.
Buchner R, Hefter GT, May PM. 1998. Dielectric relaxation of aqeous NaCl solutions. *J Phys Chem A* 103: 1–9.
Buckmaster HA. 1990. Precision microwave complex permittivity measurements of high loss liquids. *J Electromagn Waves Appl* 4: 645–656.
Bull HB, Breese K. 1969. Electrical conductance of protein solutions. *J Colloid Interface Sci* 29: 492.
Bulyshev AE, Semenov SY, Souvorov AE, Svenson RH, Nazarov AG, Sizov YE, Tatsis GP. 2001. Computational modeling of three dimensional microwave tomography of breast cancer. *IEEE Trans Biomed Eng* 48(9): 1053–1056.
Burdette EC, Friederich PG, Seaman RL, Larsen LE. 1986. *In situ* permittivity of canine brain: regional variations and postmortem changes. *IEEE Trans Microwave Theory Tech MTT* 34(1): 38–49.
Chin L, Sherar M. 2001. Changes in dielectric properties of *ex vivo* bovine liver at 915 MHz during heating. *Phys Med Biol* 46: 197–211.
Cole KS. 1972. *Membrane, Ions and Impulses*. University of California Press, Berkeley.
Cole KS, Cole RH. 1941. Dispersion and absorption in dielectrics. I. Alternating current characteristics. *J Chem Phys* 9: 341–351.
Craig DQM. 1995. *Dielectric Analysis of Pharmaceutical Systems*. Taylor & Francis, London.
Davidson DW, Cole RH. 1951. Dielectric relaxation in glycerol, propylene glycol and *n*-propanol. *J Chem Phys* 19: 1484–1490.
Debye, P., Polar Molecules, Dover, Mincola, N.Y., 1929.
Dimbylow PJ. 1996. The development of realistic voxel phantoms for electromagnetic field dosimetry. In: *Proceedings of an International Workshop on Voxel Phantom Development*, National Radiological Protection Board, Chilton, U.K., 1–7.
Dissado LA. 1990. A fractal interpretation of the dielectric response of animal tissues. *Phys Med Biol* 35(11): 1487–1503.
Dissado LA, Hill RM. 1989. The fractal nature of the cluster model dielectric response functions. *J Appl Phys* 66(6): 2511–2524.
Dobson J, Grassi P. 1996. Magnetic properties of human hippocampl tissue: evaluation of artefact and contamination sources. *Brain Res Bull* 39: 255–259.
Duck FA. 1990. *Physical Properties of Tissue: A Comprehensive Reference Book*. Academic Press, London.
Dukhin SS. 1971. Dielectric properties of disperse systems. *Surface Colloid Sci* 3: 83.
Dukhin SS, Shilov VN. 1974. *Dielectric Phenomena and the Double Layer in Disperse Systems*. John Wiley & Sons, New York.
Ellison WJ, Lamkaouchi K, Moreau J. 1996. Water: a dielectric reference. *J Mol Liq* 68: 171–279.
Epstein BR, Foster KR. 1983. Anisotropy in the dielectric properties of skeletal muscle. *Med Biol Eng Comput* 21: 51–55.

Faes TJC, Meij HA, Munk JC, Heethaar RM. 1999. The electric resistivity of human tissues (100 Hz–10 MHz) a meta-analysis of review studies. *Physiol Meas* 20: R1–R10.
Fallert MA, Mirotznik MS, Bogen DK, Savage EB, Foster KR, Josephson ME. 1993. Myocardial electrical impedance mapping of ischemic sheep hearts and healing aneurisms. *Circulation* 87: 188.
Fixman M. 1980. Charged macromolecules in external fields. 1. The sphere. *J Chem Phys* 72: 5177.
Fixman M. 1983. Thin double layer approximation for electrophoresis and dielectric response. *J Chem Phys* 78: 1483.
Foster KR. 2002. Herman P. Schwan: a scientist and pioneer in biomedical engineering. *Annu Rev Biomed Eng* 4: 1–27.
Foster KR, Schepps JL. 1981. Dielectric properties of tumor and normal tissues at RF through microwave frequencies. *J Microwave Power* 16(2): 107–119.
Foster KR, Schwan HP. 1989. Dielectric properties of tissues and biological materials: a critical review. *Crit Rev Biomed Eng* 17(1): 25–104.
Foster KR, Schwan HP. 1996. Dielectric properties of tissues. In: *CRC Handbook of Biological Effects of Electromagnetic Fields*, Polk C, Postow E, Ed., CRC Press, Boca Raton, FL pp. 25–101.
Fricke HA. 1955. A mathematical treatement of the electric conductivity and capacity of disperse systems. II. The capacity of a suspension of conducting spheroids surrounded by a nonconducting membrane for a current of low frequency. *Phys Rev* 26: 678.
Fröhlich H. 1955. *Theory of Dielectrics*. Oxford University Press, Oxford.
Gabriel C. 1997. Comments on ''Dielectric properties of the skin.'' *Phys Med Biol* 42: 1671–1674.
Gabriel C. and Gabriel S. 1997. http://www.brooks.af.mil/AFRL/HED/hedr/reports/dielectric/Report/Report.html
Gabriel C, Bentall RH, Grant EH. 1987. Comparison of the dielectric properties of normal and wounded human skin material. *Bioelectromagnetics* 8: 23–28.
Gabriel C, Gabriel S, Corthout E. 1996a. The dielectric properties of biological tissues: I. Literature survey. *Phys Med Biol* 41: 2231–2249.
Gabriel S, Lau RW, Gabriel C. 1996b. The dielectric properties of biological tissues: II. Measurements in the frequency range of 10 Hz to 20 GHz. *Phys Med Biol* 41: 2251–2269.
Gabriel S, Lau RW, Gabriel C. 1996c. The dielectric properties of biological tissues: III. Parametric models for the dielectric spectrum of tissues. *Phys Med Biol* 41: 2271–2293.
Gabriel C, Sheppard RJ, Grant EH. 1983. Dielectric properties of ocular tissues at 37°C. *Phys Med Biol* 28: 43–49.
Gabriel C., 2000. The dielectric properties of tissues. In: Radiofrequency radiation dosimetry and its relationship to the biological effects of electromagnetic fields. Editors: Klauengerg BJ and Miklavic D. Nato science series. *High Technology* (82): 75–84.
Geddes LA, Barker LE. 1967. The specific resistance of biological material—a compendium of data for the biomedical engineer and physiologist. *Med Biol Eng* 5: 271–293.
Ghodgaonkar DK, Gandhi Om P, Iskander MF. 2000. Complex permittivity of human skin *in-vivo* in the frequency band 26.5–60 GHz. *IEEE* Antennas and Propagation Society Symposium Proceedings, Salt Lake City, UT, USA, July 16–20, 2000, Vol. 2, pp. 1100–1103.
Gimsa J, Wachner D. 1998. A unified resistor–capacitor model for impedance, dielectrophoresis, electrorotation, and induced transmembrane potential. *Biophys J* 75: 1107–1116.
Gimsa J, Wachner D. 1999. A polarization model overcoming the geometric restrictions of the Laplace solution for spheroidal cells: obtaining new equations for field-induced forces and transmembrane potential. *Biophys J* 77: 1316–1326.
Gimsa J, Wachner D. 2001a. Analytical description of the transmembrane voltage induced on arbitrarily oriented ellipsoidal and cylindrical cells. *Biophys J* 81: 1888–1896.
Gimsa J, Wachner D. 2001b. On the analytical description of transmembrane voltage induced on spheroidal cells with zero membrane conductance. *Eur Biophys J* 30: 463–466.
Grant E, Shack R. 1967. Complex permittivity measurements at 8.6 mm wavelength over the temperature range 1–60 degrees centigrade. *Br J Appl Phys* 18: 1807–1814.
Grant EH, Sheppard RJ. 1974a. Dielectric relaxation in water in the neighbourhood of 4°C. *J Chem Phys* 60: 1792–1796.

Grant E, Buchanan T, Cook H. 1957. Dielectric behaviour of water at microwave frequencies. *J Chem Phys* 26: 156–161.
Grant EH, Sheppard RJ, South GP. 1978. *Dielectric Behaviour of Bilogical Molecules in Solution*. Clarendon Press, Oxford.
Grant EH, Szwarnowski S, Sheppard RJ. 1981. Dielectric properties of water in the microwave and infrared regions. In: *Biological Effects of Nonionising Radiation*, Illinger KH, Ed., American Chemical Society Symposium Series, Washington, DC, 157: 47–56.
Grant EH, McLean VER, Nightingale NRV and Gabriel C. 1984. Dielectric properties of water in biological solutions. In: *Interaction between Electromagnetic Fields and Cells*, Plessum Press, Newyork and London. Chiabrera A, Nicolini C, Schwan HP, Eds., NATO ASI Series, 97: 65–74.
Greffe JL, Grosse C. 1992. Static permittivity of emulsions. *Prog Electromagn Res* 41.
Grimnes S, Martinsen ØG, Eds. 2000. *Bioimpedance and Bioelectricity*. Academic Press, New York.
Grosse C. 1988. Permittivity of a suspension of charged spherical particles in electrolyte solution. II. Influence of the surface conductivity and asymmetry of the electrolyte on the low and high frequency relaxations. *J Phys Chem* 92: 3905–3910.
Grosse C, Foster KR. 1987. Permittivity of a suspension of charged spherical particle in electrolyte solution. *J Phys Chem* 91: 3073.
Haggis GH, Hasted JB, Buchanan TJ. 1952. The dielectric properties of water in solutions. *J Chem Phys* 20: 1452–1465.
Hagness SC, Taflove A, Bridges JE. 1998. Two-dimensional FDTD analysis of a pulsed microwave confocal system for breast cancer detection: fixed-focus and antenna-array sensors. *IEEE Trans Biomed Eng* 45(12): 1470–1479.
Hagness SC, Taflove A, Bridges JE. 1999. Three-dimensional FDTD analysis of a pulsed microwave confocal system for breast cancer detection: design of an antenna-array element. *IEEE Trans Antennas Propagat* 47(5): 783–791.
Hammerich D, Ozkan OR, Tsai JZ, Staelin ST, Tungjitkusolmun S, Mahvi DM, Webster JG. 2002. Changes in electrical resistivity of swine liver after occlusion and postmortem. *Med Biol Eng Comput* 40: 29–33.
Hanai T, Imakita T, Koizumi N. 1982. Analysis of dielectric relaxations of w/o emulsions in the light of theories of interfacial polarization. *Colloid Polym Sci* 260(11): 1029.
Hasted JB, El Sabeh. 1953. The dielectric properties of water in solutions. *Trans Faraday Soc* 49: 1003–1011.
Hasted JB, Husain SK, Frescura FAM, Birch JR. 1985. Far-infrared absorption in liquid water. *Chem Phys Lett* 118(6): 622–625.
Havriliak SJ, Negami S. 1966. A complete plane analysis of dispersion in some polymer systems. *J Polym Sci Polym Symp* 6: 99–117.
Hayashi Y, Miura N, Shinyashiki N, Yagihara S. 2005. Free water content and monitoring of healing processes of skin burns studied by microwave dielectric spectroscopy *in vivo*. *Phys Med Biol* 50: 599–612.
Hill NE, Vaughan WE, Price AH, Davies M. 1969. *Dielectric Properties and Molecular Behaviour*. Van Nostrand, London.
Hill RM, Jonscher AK. 1983. The dielectric behaviour of condensed matter and its many-body interpretation. *Contemp Phys* 24(1): 75–110.
Hwang H, Yim J, Cho J, Cheon C, Kwon Y. 2003. 110 GHz broadband measurement of permittivity on human epidermis using 1 mm coaxial probe. *IEEE MTT S Digest* 399–402.
Irimajiri A, Suzaki T, Asami K, Hanai T. 1991. Dielectric modeling of biological cells. Models and algorithm. *Bull Inst Chem Res Kyoto Univ* 69(4): 421–438.
Ishikawa A, Hanai T, Koizumi N. 1982. Dielectric properties of dextran gel Sephadex G-25 dispersed in aqueous phases. *Jpn J Appl Phys* 21(12): 1762.
Jonscher AK. 1983. *Dielectric Relaxation in Solids*. Chelsea Dielectrics Press, London.
Kaatze U. 1986. The dielectric spectrum of water in the microwave and near-millimetre wavelength region. *Chem Phys Lett* 132(3): 291–293.
Kaatze U. 1988. Complex permittivity of water as a function of frequency and temperature. *J Chem Eng* 34: 371–374.
Kaatze U. 1989. Complex permittivity of water as function of frequency and temperature. *J Chem Eng Data* 34: 371–374.

Kaatze U. 1990. On the existence of bound water in biological systems as probed by dielectric spectroscopy. *Phys Med Biol* 35(12): 1663–1681.
Kaatze U, Giese K. 1980. Dielectric relaxation spectroscopy of liquids: frequency domain and time domain experimental methods. *J Phys E: Sci Instrum* 13: 133–141.
Kent M, Peyman A, Gabriel C, Knight A. 2002. Determination of added water in pork products using microwave dielectric spectroscopy. *Food Control* 13: 43–149.
Kirkwood JG, 1936. On the Theory of Dielectric Polarization, *J Chem Phys*-Vol 4(9), 592–601.
Lahtinen T, Nuutinen J, Alanen E. 1997. Dielectric properties of the skin. *Phys Med Biol* 42: 1471–1472.
Lahtineu T, Nuntineu J, Alanen E, Turunen M, Nuortio L, Usenius T, Hopewell JW: Quantitative assessment of protein content in irradiated human skin. Int J Radiat Oncol Biol Phys 43: 635–638, 1999.
Lane JA, Saxton, JA. 1952. Dielectric dispersion in pure polar liquids at very high radio frequencies. *Proc R Soc Lond* 213: 400–408.
Latikka J, Kuurne T, Skola H. 2001. Conductivity of living intracranial tissues. *Phys Med Biol* 46: 1611–1616.
Liebe HJ, Hufford GA, Manabe T. 1991. A model for the complex permittivity of water at frequencies below 1 THz. *Int J Infrared Millimeter Waves* 12: 659–660.
Lindholm-Setson B, Han S, Ollmar S, Nicander I, Jonsson G, Lithner F, Bertheim U, Geladi P. 1998. Multivariate analysis of skin impedance data in long term type 1 diabetic patients. *Chemom Intell Lab Syst* 44: 381–394.
Mandel M, Odijik T. 1984. Dielectric properties of polyelectrolyte solutions. *Annu Rev Phys Chem* 35: 75.
Marzec E, Wachal K. 1999. The electrical properties of leg skin in normal individuals and in-patients with ischemia. *Bioelectrochem Bioenerg* 49: 73–75.
Maxwell JC. 1891. *A Treatise on Electricity and Magnetism*, 2nd ed., Vol. 1, chap. IX. Clarendon Press, Oxford.
Milton GW. 2002. *Theory of Composites*, Cambridge University Press, Cambridge.
Miyauchi T, Hirose H, Sasaki E, Hayashi M, Mori Y, Murakawa S, Takagi H, Yasuda H, Kumada Y, Iwata H. 1999. Predictability of dielectric properties for ischemic injury of the skeletal muscle before reperfusion. *J Surg Res* 86: 79–88.
Munoz San Martýn S, Sebastian JL, Sancho M, Miranda JM. 2003. A study of the electric field distribution in erythrocyte and rod shape cells from direct RF exposure. *Phys Med Biol* 48: 1649–1659.
Nicholson PW. 1965. Specific impedance of cerebral white matter. *Exp Neurol* 13: 386–401.
Nicholson C, Freeman JA. 1975. Theory of current source-density: analysis and determination of conductivity tensor for anuran cerebellum. *Neurophysiol* 38: 356–368.
Nuutinen J, Lahtinen T, Turunen M, Alanen E, Tenhunen M, Usenius T, Kolle R. 1998. A dielectric method for measuring early and late reactions in irradiated human skin. *Radiother Oncol* 47: 249–254.
Onsager L, 1936. Electric Moments of Molecules in Liquids *J. Am. Chem. Soc.* 58, 1486–1493.
Pauly H, Schwan HP. 1966. Dielectric properties and ion mobility in electrocytes. *Biophys J* 6: 621.
Petaja L, Nuutinen J, Uusaro A, Lahtinen T, Ruokonen E. 2003. Dielectric constant of skin and subcutaneous fat to assess fluid changes after cardiac surgery. *Physiol Meas* 24: 383–390.
Peters MJ, Stinstra JG, Hendriks M. 2001. Estimation of the electrical conductivity of human tissue. *Electromagnetics* 21: 545–557.
Pethig R. 1979. *Dielectric and Electronic Properties of Biological Materials*. John Wiley & Sons, New York.
Pethig R, Kell DB. 1987. The passive electrical properties of biological systems: their significance in physiology, biophysics, and biotechnology. *Phys Med Biol* 32(8): 933–970.
Pethig R. 1996. Dielectrophoresis: using inhomogeneous AC electrical fields to separate and manipulate cells. *Critical Reviews in Biotechnology* 16(4): 331–348.
Peyman A, Rezazadeh AA, Gabriel C. 2001. Changes in the dielectric properties of rat tissue as a function of age at microwave frequencies. *Phys Med Biol* 46: 1617–1629.
Peyman A, Holden S, Gabriel C. 2005. Dielectric Properties of Biological Tissues at Microwave Frequencies. Final technical report, MTHR Department of Health, U.K.

Polevaya Y, Erunolina I, Schlesinger M, Ginzburg BZ, Feldman Y. 1999. Time domain dielectric spectroscopy study of human cells II. Normal and maligant white blood cells. *Biochemic Biophysica Acta* 1419: 257–271.

Prausnitz MR, Pliquett U and Vanbever R (1999) Mechanistic studies of skin electroporation using biophysical methods in Electrically Mediated Delivery of Molecules to cells – Electrochemotherapy, Electrogenetherapy, and Transdermal Delivery by Electroporation, MJ Jaroszeski, R Gilbert, and R Heller, eds., Humana Press, Totowa, NJ, pp. 214–235.

Raicu 1999. Dielectric dispersion of biological matter: model combining Debye-type and ''universal'' response. *Phys Rev E* 60(4): 4677–4680.

Raicu V, Saibara T, Enzan H, Irimajiri A. 1998a. Dielectric properties of rat liver *in vivo*: analysis by modeling hepatocytes in the tissue architecture. *Phys Med Biol* 47: 333–342.

Raicu V, Saibara T, Irimajiri A. 1998b. Dielectric properties of rat liver *in vivo*: a non-invasive approach using an open-ended coaxial probe at audio/radio frequencies. *Phys Med Biol* 47: 325–332.

Raicu V, Kitagawa N, Irimajiri A. 2000. A quantitative approach to the dielectric properties of the skin. *Phys Med Biol* 45: L1–L4.

Ranck JB, BeMent SL. 1965. The specific impedance of the dorsal columns of cat: an anisotropic medium. *Exp Neurol* 11: 451–463.

Reynolds JA, Hough JM. 1957. Formulae for dielectric constant of mixtures. *Proc Phys Soc* 70: 769–775.

Riedel CH, Keppelen M, Nani S, Dössel O. 2003. Postmortem conductivity measurement of liver tissue using a contact free magnetic induction sensor. *EMBC IEEE* 3126–3129.

Rogers JA, Sheppard RJ, Grant EH. 1983. The dielectric properties of normal and tumour mouse tissue between 50 MHz and 10 GHz. *Br J Radiol* 56: 335–338.

Roussy G, Pearce JA. 1995. *Foundations and Industrial Applications of Microwaves and Radio Frequency Fields: Physical and Chemical Processes*. Wiley Publishers, New York.

Schaefer M, Kirlum HJ, Schlegel C, Gebhard MM. 1999. Dielectric properties of skeletal muscle during ischemia in the frequency range from 50 Hz to 200 MHHz. *Ann NY Acad Sci* 873: 59–64.

Schaefer M, Gross W, Ackemann J, Gebhard MM. 2002. The complex dielectric spectrum of heart tissue during ischemia. *Bioelectrochemistry* 58: 171–180.

Schaefer M, Gross W, Preuss M, Ackemann J, Gebhard MM. 2003. Monitoring of water content and water distribution in ischemic hearts. *Bioelectrochemistry* 61: 85–92.

Schanne OF, Ceretti ERP. 1978. *Impedance Measurements in Biological Cells*. Wiley, New York.

Schepps JL, Foster KR. 1980. UHF and microwave dielectric properties of normal and tumor tissues: variation in dielectric properties with tissue water content. *Phys Med Biol* 25: 1149–1159.

Schmid G, Neubauer G, Illievich UM, Alesch F. 2003a. Dielectric properties of porcine brain tissue in the transition from life to death at frequencies from 800 to 1900 MHz. *Bioelectromagnetics* 24: 413–421.

Schmid G, Neubauer G, Mazal PR. 2003b. Dielectric properties of human brain tissue measured less than 10 h post-mortem at frequencies from 800 to 2450 MHz. *Bioelectromagnetics* 24: 423–430.

Schwan HP. 1957. Electrical properties of tissue and cell suspensions. In: *Advances in Biological and Medical Physics*, Lawrence JH, Tobias CA, Eds., Academic Press, New York, 5: 147–209.

Schwan HP. 1992. Linear and nonlinear electrode polarization and biological materials. *Ann Biomed Eng* 20: 269–288.

Schwan HP, Foster KR. 1980. RF-field interactions with biological systems: electrical properties and biophysical mechanisms. *Proc IEEE* 68: 104–13.

Schwan HP, Sheppard RJ, Grant EH. 1976. Complex permittivity of water at 25°C. *J Chem Phys* 64: 2257–2258.

Schwartzman D, Chang I, Michele JJ, Mirotznik MS, Foster KR. 1999. Electrical impedance properties of normal and chronically infarcted left ventricular myocardium. *J Interv Card Electrophysiol* 3: 213–224.

Schwarz G. 1962. A theory of the low frequency dielectric dispersion of colloidal particles in eletrolyte solution. *J Phys Chem* 66: 2636.

Sebastian JL, Munoz S, Sancho M, Miranda JM. 2001. Analysis of the influence of the cell geometry, orientation and cell proximity effects on the electric field distribution from direct RF exposure. *Phys Med Biol* 46: 213–225.

Semenov SY, Svenson RH, Posukh VG, Nazarov AG, Sizov YE, Bulyshev AE, Souvorov AE, Chen W, Kasell J, Tatsis GP. 2002. Dielectrical spectroscopy of canine myocardium during acute ischemia and hypoxia at frequency spectrum from 100 kHz to 6 GHz. *IEEE Trans Med Imaging* 21(6): 703–707.

Sihvola AH. 1989. Self-consistency aspects of dielectric mixing theories. *IEEE Trans Geosci Remote Sensing* 27(4): 403.

Sihvola AH, Kong JA. 1988. Effective permittivity of dielectric mixtures. *IEEE Trans Geosci Remote Sensing* 26(4): 420.

Sihvola AH, Lindell IV. 1992. Polarizability modeling of heterogeneous media. *Prog Electromagn Res* PIER 06: 101–151.

Smith SR, Foster R, Wolf GL. 1986. Dielectric properties of VX-2 carcinoma versus normal liver tissue. *IEEE Trans Biomed Eng* 33(5): 522–524.

Stauffer PR, Rossetto F, Prakash M, Neuman DG, Lee T. 2003. Phantom and animal tissues for modelling the electrical properties of human liver. *Int J Hyperthermia* 19(1): 89–101.

Stuchly M. 1979. Interaction of radiofrequency and microwave radiation with living systems. *Radiat Environ Biophys* 16: 1.

Stuchly MA, Stuchly SS. 1980. Dielectric properties of biological substances—tabulated. *J Microwave Power* 15(1): 19–26.

Sunaga T, Ikehira H, Furukawa S, Shinkai H, Kobayashi H, Matsumoto Y, Yoshitome E, Obata T, Tanada S, Murata H, Sasaki Y. 2002. Measurement of the electrical properties of human skin and the variation among subjects with certain skin conditions. *Phys Med Biol* 47: N11–N15.

Surowiec AJ, Stuchly SS, Keaney M, Swarup A. 1986. *In vivo* and *in vitro* dielectric properties of feline tissues at low radio-frequencies. *Phys Med Biol* 31(8): 901–909.

Takashima S. 1989. Electrical properties of proteins. I. Dielectric relaxation. In: *Physical Principles and Techniques of Protein Chemistry*, Leach JS, Ed., Academic Press, New York.

Tamasanis D. 1992. Application of volumetric multiple scattering approximation to foliage media. *Radio Science (USA)* 27(6): 797–812.

Tamura T, Tenhunen M, Lahtinen T, Repo T, Schwan HP. 1994. Modelling of the dielectric properties of normal and irradiated skin. *Phys Med Biol* 39: 927–936.

Tinga WR. 1992. Mixture laws and microwave material interactions. *Prog Electromagn Res* 6: 1–40.

Tsai JZ, Cao H, Tungjitkusolmun S, Woo EJ, Vorperian VR, Webster JG. 2000. Dependance of apparent resistance of four-electrode probes on insertion depth. *IEEE Trans Biomed Eng* 47(1): 41–48.

Tsai JZ, Will JA, Stelle SHV, Cao H, Tungjitkusolmun S, Choy YB, Haemmerich D, Vorperian VR, Webster JG. 2002. *In-vivo* measurements of swine myocardial resistivity. *IEEE Trans Biomed Eng* 49(5): 472–483.

Van Beek LKH. 1967. Dielectric behaviour of heterogeneous systems, *Prog Dielectr* 7: 69–114.

Walker DC, Brown BH, Hose DR, Smallwood RH. 2000. Modelling the electrical impedivity of normal and prealignant cervical tissue. *Electron Lett*. 36(19): 1603–1604.

Weaver JC, Astumian RD. 1990. The response of living cells to very weak electric fields: the thermal noise limit. *Science* 247(4941): 459–462.

Wei YZ, Sridhar S. 1993. A new graphical representation for dielectric data. *J Chem Phys* 99(4): 3119–3124.

Wersebe A, Siegmann K, Krainick U, Fersis N, Vogel U, Claussen CD, Muller-Schimpfle M. 2002. Diagnostic potential of targeted electrical impedance scanning in classifying suspicious breast lesions. *Invest Radiol* 37(2): 65–72.

Woodward AM, Kell DB. 1990. On the nonlinear dielectric properties of biological systems *Saccharomyces cerevisiae*. *Bioelectrochem Bioenerg* 24: 83–100.

Yeldin M, Kwan H, Murphy JT, Nguyen-Hou H, Wong YC. 1974. Electrical conductivity in cat cerebellar cortex. *Exp Neurol* 43: 533–569.

Zaghloul H, Buckmaster HA. 1985. The complex permittivity of water at 9.356 GHz from 10 to 40 degrees C. *J Phys D: Appl Phys* 18: 2109–2118.

Zhang ZH, Sekine K, Hanai T, Koizuni N. 1983. Dielectric observations on polystrene microcapsules and the theoretical analysis with reference to interfractal polarization. *Colloid Polym Sci* 261: 381.